Grima-Cornish et al. International Journal of Mechanical and Materials Engineering (2021) 16:4
https://doi.org/10.1186/s40712-020-00125-z

International Journal of Mechanical and Materials Engineering

ORIGINAL PAPER Open Access

Mathematical modeling of auxetic systems: bridging the gap between analytical models and observation

James N. Grima-Cornish[1], Joseph N. Grima[1,2] and Daphne Attard[1*]

Abstract

The Poisson's ratio, a property which quantifies the changes in thickness when a material is stretched and compressed, can be determined as the negative of the transverse strain over the applied strain. In the scientific literature, there are various ways how strain may be defined and the actual definition used could result in a different Poisson's ratio being computed. This paper will look in more detail at this by comparing the more commonly used forms of strain and the Poisson's ratio that is computable from them. More specifically, an attempt is made to assess through examples on the usefulness of the various formulations to properly describe what can actually be observed, thus providing a clearer picture of which form of Poisson's ratio should be used in analytical modelling.

Keywords: Mechanical metamaterials, Auxetic, Negative Poisson's ratio, Poisson's function

Introduction

The link between mathematics and science is an ancient one which continues to predominate in research today. This can be attributed to the fact that mathematics gives research an angle which cannot exist with qualitative research alone, that of the removal of uncertainty in the statements and theories given. Furthermore, with the inclusion of mathematics, statements can be communicated in a factual manner which could not be done otherwise. Moreover, mathematics manages to communicate findings in a more elegant manner, which is not always the case when it is given in other ways. The elegance of mathematics is what has, in many cases, pushed forward the understanding of many subjects in science, as well as other disciplines (Russell, 1919). Famous examples, as well as everyday examples, of this can be seen practically everywhere. To name a few: high-grade commercial coffee machines are manufactured with a high level of attention and calibrated in order to produce the exact same dose of coffee at the same temperature and pressure output every time in order to completely eliminate variation from one cup of coffee to the next (Fischer & Eugster, 1994; Pandolfi, 1988); restoration of famous monuments and structures also depends greatly on mathematical models in order to get every detail correct; acoustics, such as the manufacturing of great musical halls such as the Elbphilharmonie in Hamburg (Mack, 2018), as well as manufacturing of everyday speakers for a desktop computer both involve calculations which must be made to maximise the desired effect (Juszkiewicz & Ewen, 2002), albeit one requires more perfection than the other; and the deploying of rockets and shuttles to space in order to take satellites, people and other technologies into space which require intensive mathematical calculation to a great degree of accuracy for any mission to be a success (Wilson, 1964).

This is no less important in the field of thermo-mechanical metamaterials, the field of study relating to: 'engineered materials having previously unachievable [anomalous] thermal and/or mechanical properties that are defined by their microstructural architecture rather

* Correspondence: daphne.attard@um.edu.mt
[1]Metamaterials Unit, Faculty of Science, University of Malta, Msida MSD 2080, Malta
Full list of author information is available at the end of the article

than their composition' (Zheng et al., 2014). Here, analytical modelling is used in order to break down mechanisms relating to structure down to mathematical relationships. This way, the effect of each structural variable can be looked at individually, and this information can be used to fine tune them to the required values for applications or to apply these models to other materials in order to better understand the mechanism underlying their behaviour. The above being said, a better understanding of these materials through this type of modelling allows for improvement in the designing of future applications and materials, and therefore, the overall bettering of contemporary technology in the endless search to do so.

Thermo-mechanical anomalous properties include a variety of such properties, one of which merits a particular mention is that of auxetic behaviour (Alderson et al., 2005; Alderson, Alderson, Ravirala, Simkins, & Davies, 2012; Alderson & Evans, 1992; Allen et al., 2016; Allen et al., 2017; Attard & Grima, 2012; Azzopardi, Brincat, Grima, & Gatt, 2015; Babaee et al., 2013; Baughman & Galvão, 1993; Bertoldi, Reis, Willshaw, & Mullin, 2010; Brańka, Heyes, Makowiak, Pieprzyk, & Wojciechowski, 2012; Brańka, Heyes, & Wojciechowski, 2009; Brańka, Heyes, & Wojciechowski, 2011; Dudek et al., 2017; Dudek et al., 2018; Evans, 1991; Greaves, Greer, Lakes, & Rouxel, 2011; Grima, Farrugia, Gatt, & Attard, 2008; Grima, Gatt, Alderson, & Evans, 2006; Grima, Grech, Grima-Cornish, Gatt, & Attard, 2018; Grima, Jackson, Alderson, & Evans, 2000; Ha, Plesha, & Lakes, 2016; Harkati, Daoudi, Bezazi, Haddad, & Scarpa, 2017; Hewage, Alderson, Alderson, & Scarpa, 2016; Hoover & Hoover, 2005; Ishibashi & Iwata, 2000; Kadic, Tiemo, Schittny, & Wegener, 2013; Kolken & Zadpoor, 2017; Lakes, 1987; Lim, 2013; Lim, 2015; Liu & Hu, 2010; Mizzi et al., 2018; Pasternak & Dyskin, 2019; Poźniak, Wojciechowski, Grima, & Mizzi, 2016; Qin, Sun, Liu, Li, & Liu, 2017; Qu, Kadic, Naber, & Wegener, 2017; Ryder & Tan, 2016; Sigmund, 1995; Strek, Maruszewski, Narojczyk, & Wojciechowski, 2008; Strek, Michalski, & Jopek, 2019; Taylor et al., 2014; Tretiakov & Wojciechowski, 2014; Verma, Shofner, & Griffin, 2014; Verma, Shofner, Lin, Wagner, & Griffin, 2015; Wojciechowski, 1987; Wojciechowski, 1989; Wojciechowski, 2003a; Wojciechowski, Tretiakov, & Kowalik, 2003; Zhang, Hu, Liu, & Xu, 2013). Auxetic behaviour, or auxeticity, is the property which describes a material becoming fatter when stretched and thinner when compressed (Evans, Nkansah, Hutcherson, & Rogers, 1991). This anomalous property manifests when the material or structure has what is known as a negative Poisson's ratio as described in more detail below. Since the coining of the term by Evans et al. (1991), numerous materials have been found or been designed to manifest this property, including foams, nanolayers, crystals and constructible macrostructures.

It has long been recognised that one of the best methods to study auxetics and related systems is via the formulation of mathematical models. A typical approach involves the representation of the salient geometric features of a material through a structural model and to then analyse the deformation mechanism afforded by this model structure. The success of this approach lies partly in the fact that auxeticity requires the right synergism between 'geometry' and 'deformation mechanism' (Alderson & Evans, 1995; Grima, Alderson, & Evans, 2005), but also due to the fact that, as stated above, a mathematical model can depict a system in an unequivocal manner which removes shadows of uncertainty.

This being said, there is an issue which is so far grossly unresolved: how to compute the Poisson's ratio in a meaningful and practical manner which can adequately be used for the derivation of mathematical models as well as to report experimental data. Such Poisson's ratio should be able to clearly describe the behaviour of the system, without overlooking or over-emphasising some critical aspects of the system. This in turn poses a question how strain should be reported, a problem that is particularly pertinent in the field of auxetics when, during uniaxial loading, there is a 'non-standard' response to loads. Circumstances which offer such a challenge include, for example, situations when during stretching, the sample would initially be visibly getting thinner and then, past a certain amount of stretching, the sample starts to get 'fatter'. This problem is amply discussed by Smith, Wootton, and Evans (1999) where recommendations were made on how experimental data should be analysed and reported so as to bring to light the auxetic properties of the test sample. The present work will look at the other side of this issue, that is, how it is best to perform and report mathematical models in a meaningful and elegant manner which is easy to correlate to experimental work and at the same time does not output Poisson's ratios which look highly fascinating (e.g. gigantic auxeticity) but are mere artefacts of the reporting protocol used. This will be performed in a manner which explains, step-by-step, how analytical modelling of simple systems can be performed by looking at two of the more well-known models for mechanical metamaterials, namely the hexagonal honeycomb (Abd El-Sayed, Jones, & Burgess, 1979; Evans, Alderson, & Christian, 1995; Gibson, Ashby, Schajer, & Robertson, 1982; Masters & Evans, 1996) deforming through changes in angle (i.e. idealised hinging model as considered by (Evans et al., 1995; Masters & Evans, 1996) and the rotating rectangles model (Type I, (Grima, Alderson, & Evans, 2004; Grima, Alderson, & Evans, 2005)).

Methods

Methods used for calculation of discrete strains and Poisson's ratios

The Poisson's ratio of a sample is a property which measures the extent of change in lateral dimensions in some particular cross-section, for a given direction of uniaxial stretching in the same cross-section. The accepted convention for the reporting of the Poisson's ratio requires the identification of these directions. In fact, for a 3D sample of measurements X, Y and Z in the x-, y- and z-directions, respectively, the Poisson's ratio in the Ox_1-Ox_2 plane for uniaxial stretching in the Ox_2 direction is defined as, ν_{21}, where ν_{21} can be determined as follows:

$$\nu_{21} = -\frac{\text{Resultant strain in lateral } Ox_1 \text{ direction}}{\text{Applied axial strain in } Ox_2 \text{ direction}} = -\frac{\varepsilon_1}{\varepsilon_2}$$

where ε_2 represents the applied uniaxial strain being applied in the Ox_2 direction whilst ε_1 represents the strain in the perpendicular Ox_1 direction, i.e. a direction which is orthogonal to that where the uniaxial stain is being applied and which must lie in the plane where the Poisson's ratio is measured. The order of suffixes for the Poisson's ratio is important, where the first suffix by convention refers to the direction of stretching (i.e. corresponds to the strain in the denominator). The negative sign ensures that the vast majority of materials which tend to get thinner (–ve ε_1) when stretched (+ve ε_2) would have a positive Poisson's ratio. The Poisson's ratio is one of the fundamental mechanical properties and can range from $-1 \le \nu \le +0.5$ for three-dimensional isotropic materials (Lempriere, 1968), $-1 \le \nu \le +1$ for two dimensional materials (Wojciechowski, 2003b) and can take any value for anisotropic materials (Wojciechowski, 2003b).

The problem that arises is that, whilst there is uniformity in how the Poisson's ratio is determined from strains, there are various accepted conventions on how strains can be reported, which unfortunately would result in very distinct forms of the Poisson's ratio. To illustrate this, one may refer to an arbitrary linear system of original length $L_{init} = L[0]$ which is being stretched and re-measured n successive times such that the new lengths are $L[1]$, $L[2]$, $L[3]$, …, $L[n]$ till reaching a final length $L_{fin} = L[n]$. These length measurements are given by (see Fig. 1 for definition of terms, noting that $\delta L[i]$ refers to the change in L with respect to the previous length and $\Delta L[i]$ refers to the total change in L with respect to L_{init}):

$$\begin{aligned}
&L[0] = L_{init}\\
&L[1] = L[0] + \delta L[1] = L_{init} + \delta L[1] = L_{init} + \Delta L[1]\\
&L[2] = L[1] + \delta L[2] = L_{init} + \delta L[1] + \delta L[2] = L_{init} + \Delta L[2]\\
&L[3] = L[2] + \delta L[3] = L_{init} + \delta L[1] + \delta L[2] + \delta L[3] = L_{init} + \Delta L[3]\\
&\ldots\\
&L[k] = L[k-1] + \delta L[k] = L_{init} + \sum_{i=1}^{k} \delta L[k] = L_{init} + \Delta L[k]\\
&\ldots\\
&L[n] = L[n-1] + \delta L[n] = L_{init} + \sum_{i=1}^{n} \delta L[n] = L_{init} + \Delta L[n] = L_{fin}
\end{aligned}$$

Obviously, this type of experiment could also have been carried out in compression. From these successive

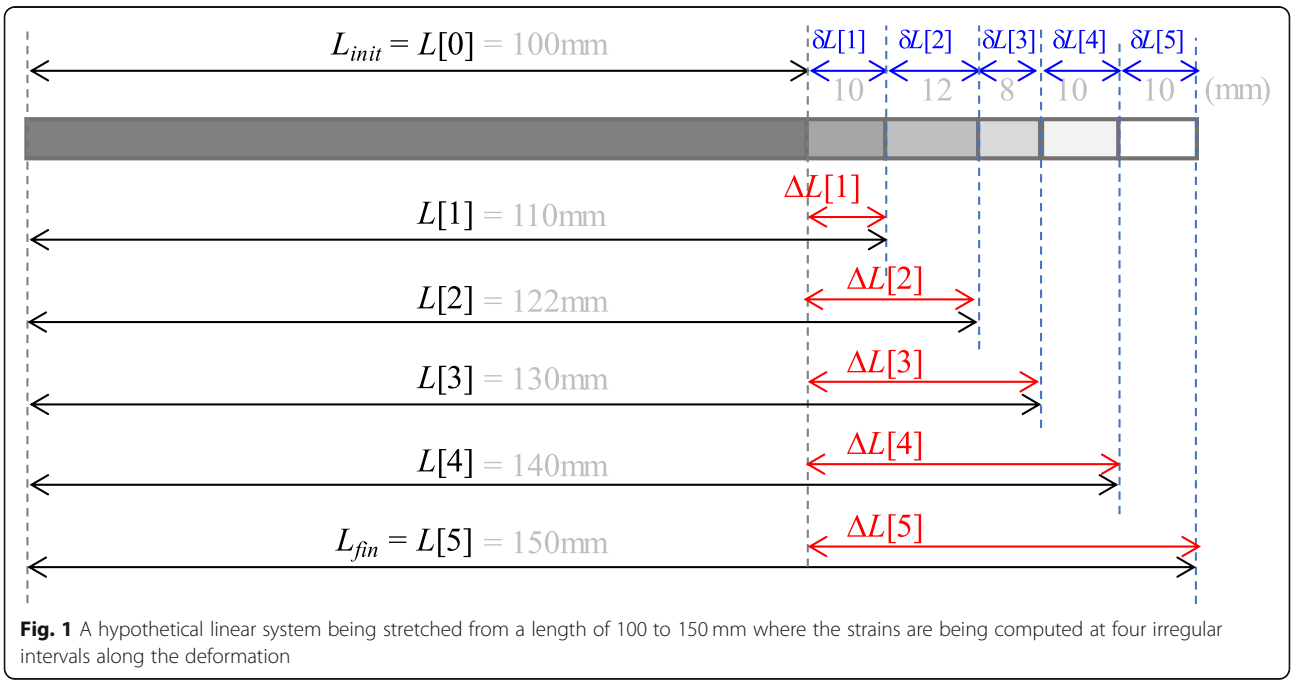

Fig. 1 A hypothetical linear system being stretched from a length of 100 to 150 mm where the strains are being computed at four irregular intervals along the deformation

measurements, which could have easily been recorded in an experimental procedure, as noted by Smith et al. (1999), one may compute strain in a number of ways including the following:

(a) The 'engineering strain', also commonly referred to as the Cauchy strain or the nominal strain, the strain which is most widely used by the engineering and experimental community which is reported as the ratio of the 'extension over the original' length, defined at point k as follows:

$$e^{eng}[k] = \frac{\Delta L[k]}{L_{init}}$$

This strain is also sometimes expressed as a percentage. The Poisson's ratio computed using such strain is normally referred to as the 'engineering Poisson's ratio'.

(b) The 'instantaneous strain', also sometimes referred to as the 'incremental strain' where for any two successive length measurements, the strain at point k is defined as follows:

$$\delta\varepsilon[k] = \frac{L[k] - L[k-1]}{L[k-1]} = \frac{\delta L[k]}{L[k-1]}$$

which strain, in the limit of infinitesimal δL, will become equivalent to the strain normally used in the derivation of analytical models, commonly referred to as the 'infinitesimally small strain' defined as follows:

$$d\varepsilon = \frac{dL}{L} = \lim_{\delta L[k]\to 0}\left(\frac{\delta L[k]}{L[k-1]}\right)$$

The Poisson's ratio computed using such strain is sometimes referred to as the 'Instantaneous Poisson's ratio' or the 'Poisson's Function'.

(c) The 'true strain', also commonly referred to as the Hencky strain, or, logarithmic strain, defined at point k as follows:

$$\begin{aligned} e^{true}[k] &= \int_{L[0]}^{L[k]} d\varepsilon = \int_{L[0]}^{L[k]} \frac{dL}{L} \\ &= [\ \ln(L)]_{L[0]}^{L[k]} = \ln(L[k]) - \ln(L[0]) = \ln\left(\frac{L[k]}{L[0]}\right) \\ &= \ln\left(\frac{L[0] + \Delta L[k]}{L[0]}\right) = \ln\left(1 + \frac{\Delta L[k]}{L[0]}\right) = \ln(1 + e^{eng}) \end{aligned}$$

The Poisson's ratio computed using such strain is sometimes referred to as the 'true Poisson's ratio'.

Methods used for calculation of the Poisson's ratio properties of periodic systems

This section presents a step-by-step guide for evaluating the Poisson's ratios of periodic 2D systems, exemplified through the hinging honeycomb system using the different methods stated above in a manner which can be easily reproduced and extended using the other models. This will be followed by the reporting of the equivalent expressions for strains and Poisson's ratios derived with the same procedures. These expressions for the Poisson's ratio based on the different methods to compute strain may hence be compared so as to assess their relative ability to describe the behaviour upon uniaxial loading well, in particular the Poisson's ratio. This process will then be repeated for the type I rotating rectangles system, so as to further illustrate the methodology and the concepts presented.

Hexagonal honeycombs

Over the years, there have been various studies on the re-entrant and non-re-entrant honeycomb system so as to study their mechanical behaviour, where deformation is typically assumed to be trough flexure of the ligaments (Abd El-Sayed et al., 1979; Evans et al., 1995; Gibson et al., 1982; Masters & Evans, 1996) or changes in angles between the ligaments, i.e. as an idealised hinging model (Evans et al., 1995; Masters & Evans, 1996). The honeycomb model structure, like many others studied for similar purposes, can be described as a finite system containing a finite number of honeycomb cells, or, as an infinity of cells where a 'representative repeat unit' is tessellated to form a space-filling model. The latter representation is normally being the preferred version, for various reasons ranging from mathematical elegance in the model to their ability to represent nano- or mirco-scale honeycombs where the number of cells present in a real sample is so large that it can be treated like an infinitely large system. The methodology applied in the formulation and derivations of such models typically involves the following:

(a) Definition of the 'research problem' and identification of what needs to be studied;
(b) Definition of the *geometry* of the system in a manner where every independent length and angle is uniquely identified, including the identification of a suitable periodically repeating unit (the 'unit cell');
(c) Formulation of the assumption related to the *deformation mechanism* and identification of the geometric parameters which will be treated as the variables and those that will be assumed to be constant (depending on the deformation mechanism);

(d) Expression of the unit cell parameters in terms of geometric parameters and variables;
(e) Calculation of strains from the unit cell parameters and formulation of expressions for the Poisson's ratio (and other relevant properties).

Definition of the research problem Any model for a given system, irrespective of how simple the system may look, is never likely to be fully comprehensive given the various aspects that one could study. In this particular case, it needs to be stated a priori that the aim of this study is to represent the deformations and properties of the system depicted in Fig. 2 in a mathematical manner, i.e. describe what happens as the system is being pulled or compressed either in the direction along the length of the vertical ligaments, or in the orthogonal direction, as depicted, and where deformations only occur through in-plane changes in angle. Whilst this statement may look trivial, it excludes the need to over define the system and can be used as a guide to appropriately select between different possible methods of definition or simplification, as indicated in more detail below. For example, by stating that only the mechanical aspects related to uniaxial loading are being studied, one may automatically preclude, for example, the need to consider any possible thermal, electrical and magnetic effects on the system.

Definition of the geometry The system under study is described graphically in Fig. 2 and may be described as a two-dimensionally periodic structure, where in simple terms, a periodic structure is defined as a system made from sub-structural units which are tessellated in one-dimension, two-dimensions or three-dimensions in a space filling manner. Examples of one-dimensional periodic structures include railway tracks (or, in mathematics, the trigonometric functions) whilst crystals are probably the best well-known examples of systems exhibiting three-dimensional periodicity. Examples of two-dimensional periodic systems, apart from the honeycombs studied here, include some of the well-known patterned/Islamic tiling designs.

To adequately describe the geometry of this periodic system, one should first attempt to identify the appropriate 'unit cell' which may be used to generate the full system through tessellation (i.e. via translation only). As

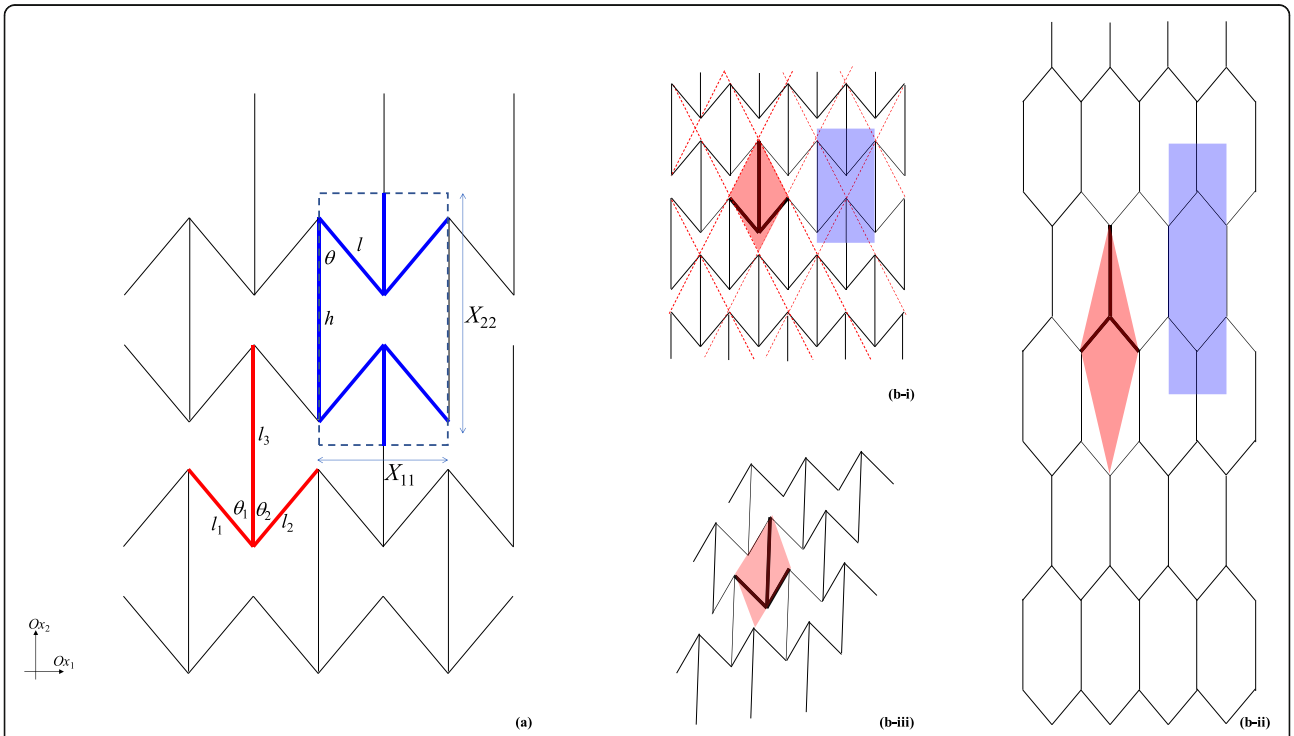

Fig. 2 The system being modelled which in general could have non-equal lengths and non-equal angles, but in this case, it shall be assumed that the system will have $l_1 = l_2 = l$ and $l_3 = h$ (kept constant), and $\theta_1 = \theta_2 = \theta$ (a variable). For the purpose of this study, the system will only be uniaxially loaded in the vertical Ox_2 direction and the ligaments will not be allowed to stretch, flex or move out of plane, i.e. θ is the only variable. Note that the parameters are defined in (**a**) whilst (**b**) shows various representations with the possible unit cells identified where (b-i) shows a re-entrant system, (b-ii) shows a non-re-entrant conventional honeycomb and (b-iii) shows a sheared system (or an irregular non-symmetric honeycomb). All of these conformations can be represented by the unit cells. Note that the convention being used to label θ is not the same as that used in previous work by (Abd El-Sayed et al., 1979; Evans et al., 1995; Gibson et al., 1982; Masters & Evans, 1996)

illustrated in Fig. 2b, the smallest unit cell which may be used to describe these hexagonal honeycombs is the one highlighted in red which contains just three ligaments. This smallest unit cell is in the shape of a parallelogram for sheared systems, which becomes rhombic when the angles between the ligaments are made equal (a result of the added symmetry). Whilst, in theory, this smallest unit cell can be used to derive the mathematical models of the system, in practice, it is much more convenient to choose a larger rectangular-shaped unit cell which has the advantage that for non-sheared systems, such as the ones modelled here, the unit cell angles are 90° and one of its unit cell vectors is parallel to the ligaments of length h. As a result, when modelled with this rectangular unit cell, the structure may easily and elegantly be aligned with the Cartesian axis, as shown in Fig. 2.

Having identified these unit cells, the next step is to identify the essential geometric parameters that are needed to describe the whole system. As noted above, availability of the parallelogram-shaped unit cells dictates that the whole system, in general, can be generated through tessellation of just three ligaments of length l_1, l_2 and l_3 joined together at their end and two angles θ_1 and θ_2 (the third angle is $360^o - (\theta_1 + \theta_2)$, due to the construing of planar Euclidean geometry). Here, it should be noted that, for this particular case, the system studied (the original undeformed system) is further assumed to have lengths $l_1 = l_2 = l$ and $l_3 = h$, and angles $\theta_1 = \theta_2 = \theta$. However, at this stage, without looking at the permitted deformation mechanism/s, one cannot assume that the condition of equality will remain valid throughout the deformation.

Definition of the deformation mechanism Having described the general case and the geometric parameters which are needed to describe the system, one should attempt to reduce the number of variables by looking at the 'deformation mechanism' and formulating the appropriate assumptions to be used. In this particular case, as noted above, it is being assumed that deformations occur only through changes in the angles between the ligaments, i.e. an idealised hinging model. This precludes any changes in length and it may thus be assumed that the lengths $l_1 = l_2 = l$ and $l_3 = h$ remain constant throughout the deformation process. This means that the lengths l and h are not to be treated as variables but as simple geometric parameters which are used to define the shape and size of the structure, but which remain constant in the deformation (idealised hinging model).

It is also assumed that this particular derivation will only look at uniaxial loading in the vertical Ox_2 direction, or, the horizontal Ox_1 direction. In general, the two angles θ_1 and θ_2 are independent of each other, and if the system had to be subjected to shear loading or off-axis loading, which is not the case in this work, $\theta_1 \neq \theta_2$. However, if what is being considered is a particular scenario where two ligaments are (and remain) of equal length l, the honeycombs angles are initially at an equal magnitude $\theta_1 = \theta_2$. Additionally, if the system is only being subjected to uniaxial on-axis loading for the rectangular unit cell (i.e. loading in the Ox_1 or Ox_2 direction), the angles θ_1 and θ_2 remain equal to each other due to symmetry. Hence, it may be further assumed that $\theta_1 = \theta_2 = \theta$, which is the only variable of this system. In other words, given that as noted above, the scope of this modelling exercise is to study uniaxial loading in the Ox_1 or Ox_2 directions where the ligament lengths do not change, for the purpose of this work, it is sufficient to define the geometry in terms of three parameters: the lengths l and h, and the angle θ, of which only θ is a variable.

Here, it must be emphasised that this condition, which provides the simplification that for uniaxial on-axis loading $\theta_1 = \theta_2 = \theta$, only holds for on-axis loading and there is no actual physical constrain to force these angles to remain equal. In fact, had the system sheared, these angles will no longer remain of equal value. This is in sharp contrast with other 'rotating squares' (Grima & Evans, 2000), 'rotating rectangles' (Grima et al., 2004; Grima, Gatt, Alderson, & Evans, 2005; Grima, Manicaro, & Attard, 2011) or other unimode systems typically studied by Milton (2013), since this condition only applies if loading is on-axis. However, this honeycomb system can be transformed to a more constrained system by letting $h = 0$, which would transform the 'hinging honeycomb' to a 'wine-rack' model.

Expression of cell parameters and alignment in space Having identified the unit cell/s that could be used for defining the system, and the geometric parameters/variables needed to fully describe the system to be modelled, the alignment of the system in the global space needs to be defined, and the unit cell parameters measured in terms of these geometric parameters/variables.

As amply described in standard crystallography textbooks, in general, any periodic 3D systems (such as crystals) can be described in terms of a unit cell in the shape of a parallelepiped which, in turn, can be described in terms of three vectors which correspond to the sides of the unit cell. By convention, these three vectors are denoted by **a**, **b** and **c** which have a length a, b and c, respectively. The angles between these cell vectors (the unit cell angles) are denoted as α (the angle between b and c), β (the angle between a and c) and γ (the angle between a and b). Whilst in general, this unit cell (and hence the crystal) can be aligned in the 3D global space in an arbitrary manner, as per convention proposed by the Institute of Radio Engineers (IRE) [Mason, 1950],

the crystal is typically aligned in space with the **c** cell vector always parallel to the Ox_3-direction (i.e. its components in the Ox_1 and Ox_2 direction are 0); the **b** cell vector always lying in the Ox_2-Ox_3 plane (i.e. its component in the Ox_1 direction is 0) and the remaining **a** vector left free in space. With this alignment, the cell vectors are of the following forms:

$$\mathbf{a} = (X_{11}, X_{12}, X_{13})$$
$$\mathbf{b} = (0, X_{22}, X_{23})$$
$$\mathbf{c} = (0, 0, X_{33})$$

i.e. the system will always have its unit cell projections in the Ox_1, Ox_2 and Ox_3 directions as X_{11}, X_{22} and X_{33}. This offers significant simplification in calculating strains.

For the simpler 2D system, a similar type of alignment is normally used, where the unit cell is aligned in the plane with one of its sides aligned parallel with the Ox_2 axis and the other side left free. Thus, for a parallelogrammical unit cell, referring to Fig. 3, the cell vectors would be of the form **a** = (X_{11}, X_{12}) and **b** = (0, X_{22}) with the special case of a rectangular unit cell having **a** = (X_{11}, 0) and **b** = (0, X_{22}), where X_{11} and X_{22} are the projections of the unit cell in the Ox_1 and Ox_2 on-axis directions, respectively.

In the particular case of the honeycomb, as discussed above, it is possible and convenient to formulate the model in terms of a rectangular unit cell, where, referring to Fig. 2, the shape and size of the representative unit cell of this hexagonal honeycomb may be described quantitatively by the unit cell projections in the Ox_1 and Ox_2 directions as follows:

$$X_{11} = 2l\ \sin\theta$$

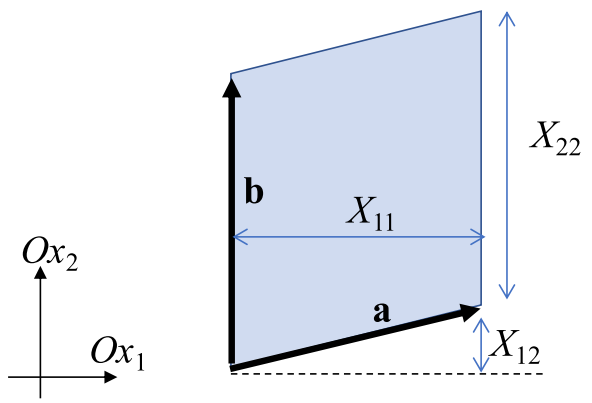

Fig. 3 Alignment of a 2D unit cell in the Cartesian space based on the convention adopted by the Institute of Radio Engineers (IRE) as specified in Mason (1950)

$$X_{22} = 2(h - l\ \cos\theta)$$

Note that with θ as defined here, angles of $0^o < \theta < 90^o$ would correspond to re-entrant honeycombs, angles $90^o < \theta < 180^o$ would correspond to conventional non re-entrant honeycombs and $\theta = 90^o$ would correspond to the special case of a honeycomb having T-shaped junctions.

Strains and Poisson's ratios Given the expressions for X_{ii} as a continuous function of a single variable, the angle θ, one may derive expressions for strains which can be considered as being the continuous equivalent of the discrete strains presented above. Throughout this derivation, recognising that the formulation of the engineering strain and true strain require and are dependent upon the identification of a starting 'original' conformation of the system, it shall be assumed that unless otherwise stated, the deformation will be performed on a honeycomb which is characterised by angle θ_0 between the ligaments such that the original undeformed conformation is represented by a unit cell of dimensions $X_{11}(\theta_0) \times X_{22}(\theta_0)$.

With this in mind, for $X_{ii} = X_{ii}(\theta)$, the engineering, infinitesimal and true strains in the Ox_i directions can be defined, respectively as follows:

$$e_i^{eng}(\theta) = \frac{X_{ii}(\theta) - X_{ii}(\theta_0)}{X_{ii}(\theta_0)} = \frac{X_{ii}(\theta)}{X_{ii}(\theta_0)} - 1$$

$$d\varepsilon_i(\theta) = \frac{dX_{ii}}{X_{ii}} = \frac{1}{X_{ii}}\frac{dX_{ii}}{d\theta}d\theta$$

$$e_i^{true}(\theta) = \int_{X_{ii}(\theta_o)}^{X_{ii}(\theta)} \frac{1}{X_{ii}} dX_{ii} = [\ \ln(X_{ii})]_{X_{ii}(\theta_o)}^{X_{ii}(\theta)}$$
$$= \ln(X_{ii}(\theta)) - \ln(X_{ii}(\theta_0)) = \ln\left(\frac{X_{ii}(\theta)}{X_{ii}(\theta_o)}\right)$$

where the respective Poisson's ratios, as a function of θ, are hence given as follows:

$$\nu_{ij}^{eng}(\theta) = -\frac{e_j^{eng}(\theta)}{e_i^{eng}(\theta)} = -\left(\frac{X_{jj}(\theta) - X_{jj}(\theta_0)}{X_{ii}(\theta) - X_{ii}(\theta_0)}\right)\frac{X_{ii}(\theta_0)}{X_{jj}(\theta_0)}$$

$$\nu_{ij}^{f'n}(\theta) = -\frac{d\varepsilon_j(\theta)}{d\varepsilon_i(\theta)} = -\frac{X_{ii}}{X_{jj}}\left(\frac{dX_{jj}}{d\theta}\right)\left(\frac{dX_{ii}}{d\theta}\right)^{-1}$$

$$\nu_{ij}^{true}(\theta) = -\frac{e_j^{true}(\theta)}{e_i^{true}(\theta)} = -\ln\left(\frac{X_{jj}(\theta)}{X_{jj}(\theta_o)}\right)\Big/\ln\left(\frac{X_{ii}(\theta)}{X_{ii}(\theta_o)}\right) = -\frac{\ln\left(X_{jj}(\theta)\right) - \ln\left(X_{jj}(\theta_0)\right)}{\ln\left(X_{ii}(\theta)\right) - \ln\left(X_{ii}(\theta_0)\right)}$$

where the expressions can be plotted against the geometric variable, or, probably more practically for real applications, against the applied engineering strain or the applied true strain so as to obtain the strain-dependent Poisson's ratio. The latter plots would need to be obtained in a parametric manner.

The type I rotating rectangles model

The same approach was applied to the type I rotating rectangles model. In this case, it may be shown that, although the smallest unit cell is one which contains just two rectangles, it is much more convenient to model the structure through the rectangular unit cell shown and defined in Fig. 4. The unit cell projections in the Ox_1 and Ox_2 directions are given as follows:

$$X_{11} = 2\left[a\cos\left(\frac{\theta}{2}\right) + b\sin\left(\frac{\theta}{2}\right)\right]$$

$$X_{22} = 2\left[a\sin\left(\frac{\theta}{2}\right) + b\cos\left(\frac{\theta}{2}\right)\right]$$

where in this case, if the rectangles are assumed to be perfectly rigid and simply rotate relative to each other in the plane of the structure, the system fulfils all the requirement to be a unimode mechanism where, for a given a and b, the structural properties are fully defined through the angle θ (the only variable during deformation).

Results and discussion

Comparison of the different methods for computing strain and Poisson's ratios

Without loss of generality, the different methods for computing strains are illustrated for the system shown in Fig. 1 for $n = 5$ where a wire-like system is stretched from an initial length of $L_{init} = L[0] = 100$ mm to a final length $L_{fin} = L[5] = 150$ mm, in successive increments of $\delta l[k] = 10$ mm, 12 mm, 8 mm, 10 mm and 10 mm. The calculated strains using the different methods are given in Table 1. These very simple calculations highlight three important characteristics, which might sound trivial, but are worth stating:

(i) The engineering strain, particularly when expressed as a percentage, is useful to provide a very visual representation of the deformation in a cumulative manner: indeed, it is easy to visualise that the final length is 50% longer than the starting length, a feature which no other strain measurement can provide;
(ii) The 'instantaneous strain' and the 'true strain' can highlight the fact that the 10 mm increases in length are not all equivalent: as the system is stretched longer, successive 10 mm increases will contribute to a smaller relative extension when compared to earlier ones when the length was shorter;
(iii) Only the engineering or true strains provide a cumulative measure, one which could be used, for example, to plot stress-strain curves, this being an obvious consequence of the manner how the 'instantaneous strain' is calculated.

Nevertheless, the distinction between the three different methods of computing the strain becomes more

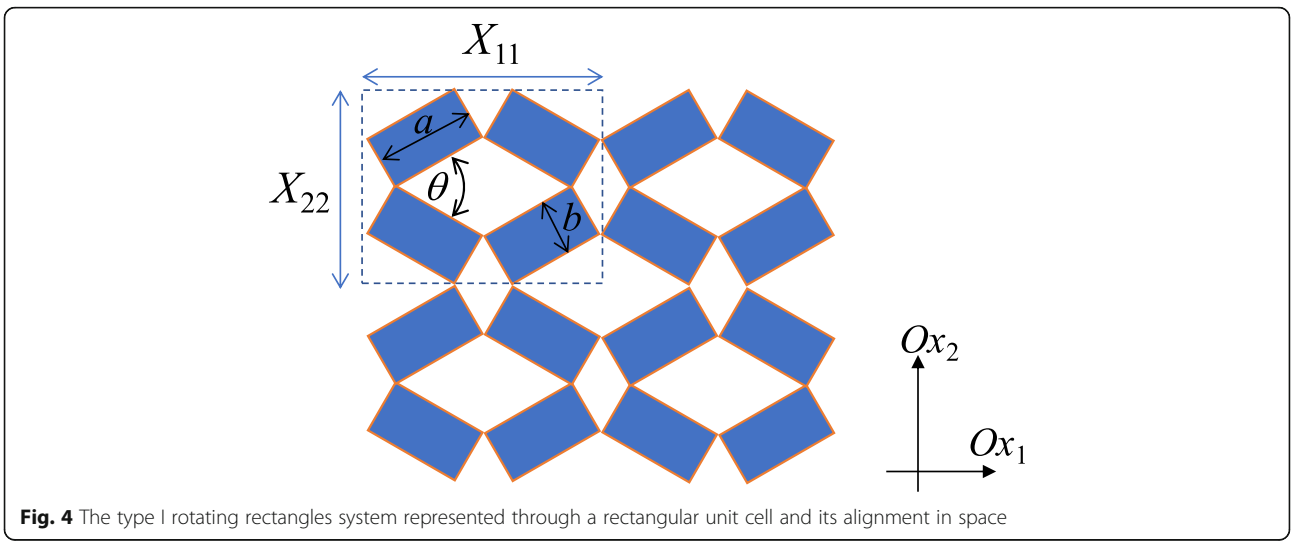

Fig. 4 The type I rotating rectangles system represented through a rectangular unit cell and its alignment in space

Table 1 The linear dimensions of the system in Fig. 1 and the calculated engineering strain, the engineering strain as a percentage, the instantaneous strain and the true strain

k	$L[k]$	$\delta L[k]$	$\Delta L[k]$	e^{eng}	e (%)	$\delta\varepsilon$	e^{true}
0	100	0	0	0.000	0	0.000	0.000
1	110	10	10	0.100	10	0.100	0.095
2	122	12	22	0.220	22	0.109	0.199
3	130	8	30	0.300	30	0.066	0.262
4	140	10	40	0.400	40	0.077	0.336
5	150	10	50	0.500	50	0.071	0.405

evident when used to compute the Poisson's ratio. Once again, without loss of generality, these different methods for computing strains and Poisson's ratios are illustrated in Fig. 5a for a system based on nine measurements (see Table 2), these being labelled A-I. Here, the system is being stretched in the vertical Ox_2 direction so its height changes from X_{22} = 30 mm to X_{22} = 62 mm. As this is happening, the width X_{11} of the system in the Ox_1 direction is initially decreasing as the system gets thinner (from A to C), then its width X_{11} remains constant (from C to D), and then X_{11} increases (from D to H) in such a manner that system F has the same width as the original system A, with systems G and H having a width which is larger than system A. The width X_{11} of the system then decreases again (from H to I) in such a manner that system I has a smaller width X_{11} than system H, which width is still larger when compared to that of the original system A.

The strains and Poisson's ratios computed through the different methods are reported in Table 2 and plotted in Fig. 5c against the vertical height Y and the engineering strain. From these results, taking system A as the initial system, it is evident that the reported Poisson's ratio is very much dependent on the manner how the strains are computed. Of the three methods, it is only the instantaneous Poisson's ratio that could capture the observation that there was no change in width upon stretching from X_{22} = 38 to X_{22} = 42 mm (C to D), something which would correspond to zero Poisson's ratio. Similarly, the very evident auxeticity which is demonstrated as the system is stretched from X_{22} = 42 mm is not captured by the engineering Poisson's ratio and the true Poisson's ratio, since between X_{22} = 42 mm and X_{22} = 50 mm (D to F), the width of the system would be smaller or equal to that of the original sample. All three methods of calculating Poisson's ratio report auxeticity when stretched beyond X_{22} = 50 mm till X_{22} = 58 mm, as expected, but only the instantaneous Poisson's ratio could capture the non-auxetic characteristics on stretching from X_{22} = 58 mm till X_{22} = 62 mm (H to I). From this perspective, one could easily conclude that the Poisson's ratio computed from the instantaneous strains is superior to the other methods. However, whilst from a purely scientific perspective, one cannot contradict the fact that the system is auxetic as it is stretched from X_{22} = 42 mm onwards, it should be equally recognised that from a practical perspective, the evident auxeticity in the region between X_{22} = 42 to X_{22} = 50 mm could well be useless. In fact, from a practical perspective it is only the widening compared to the initial system which is of important result since in a number of practical situations, it is only 'before' and 'after' states which matter, and not the path taken during the deformation. An example of this would be in devices such as rivets where, for proper affixation, the width would need to be larger than the original. Such information can be more easily obtained from the engineering Poisson's ratio or the true Poisson's ratio, since the system where the width would have once again reached that of the original sample (system F, X_{22} = 50 mm) would have an engineering or true Poisson's ratio of zero, beyond which auxeticity is reported. Unfortunately, this important information, at least from a practical perspective, is not easy to extrapolate from the data relating to the instantaneous Poisson's ratio as there is nothing remarkable about the instantaneous Poisson's ratio of system F. It should also be noted that although the system was not behaving in an auxetic manner as it was stretched from X_{22} = 58 to X_{22} = 62 mm (H to I), its width is still larger than that of the original sample, something which is not identifiable from the instantaneous Poisson's ratio.

However, it is equally true that knowledge of Poisson's ratio during the deformation path could be important in other practical applications. For example, had the application been a cable passing through a hole, where the sample is pulled from an initial length to a final length, and in the process change the thickness to an appropriate final thickness, knowledge of the dimensional changes as the sample is stretched would have been of paramount importance, for instance, so as to ensure that the thickness achievable through the deformation process would always be smaller than the hole the cable is passing through. Similarly, in applications where the sample needs to be "seen" getting fatter as it is stretched, then the only usable portion of the deformation would be that where the instantaneous Poisson's ratios give a negative Poisson's ratio (or positive if the sample needs to be 'seen' getting thinner).

At this point, it should be noted that the engineering and true Poisson's ratios are particularly sensitive to the choice of the initial system. In fact, very different results would have been obtained if, for example, system D is chosen as the initial structure. In this case, since system C corresponds to a conformation which represents the

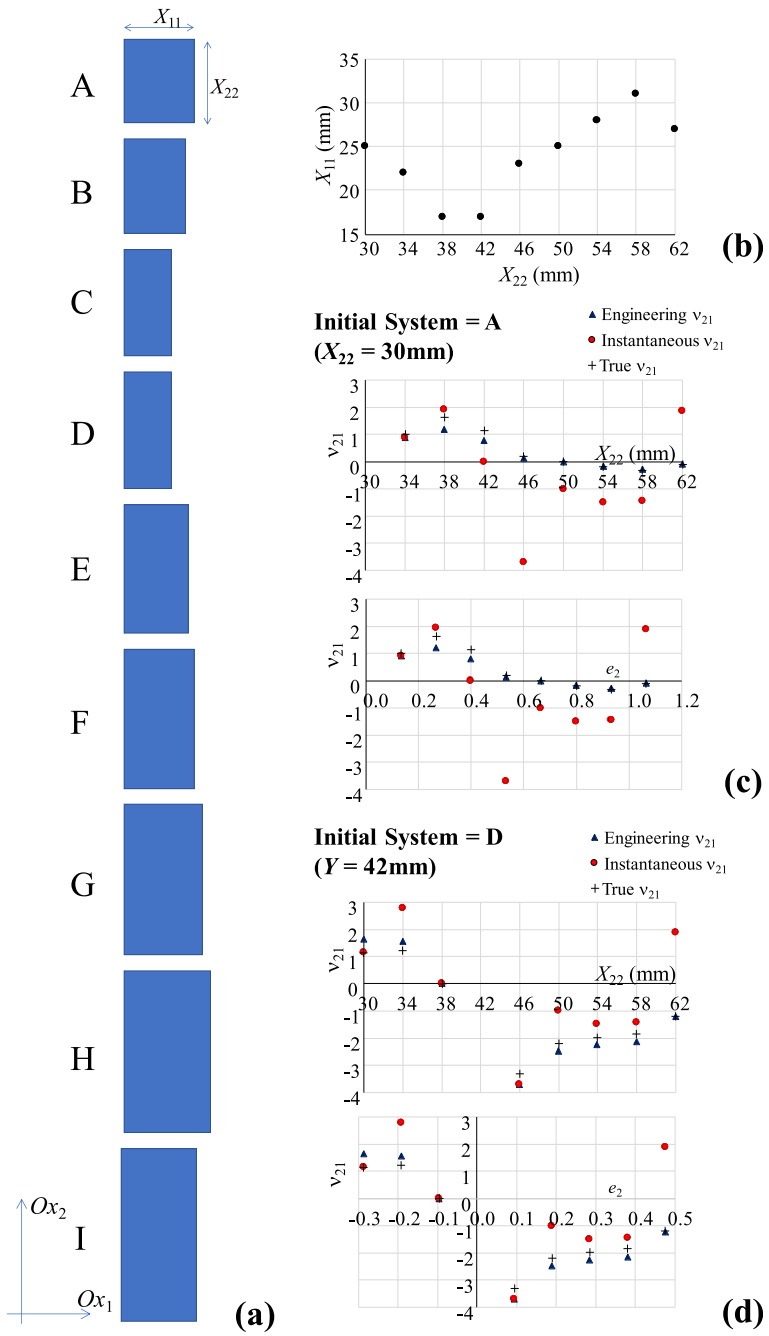

Fig. 5 a A hypothetical 2D system being stretched from a length of 30 to 62 mm in the vertical direction; **b** plot of the width vs the length, **c**, **d** plots of the Poisson's ratios vs. length or engineering strain, with the initial system being A for **c** and D for **d**

main 'turning point' in the behaviour, there is much less disagreement between the different formulations of the Poisson's ratio. Nevertheless, it must be emphasised that for real samples, the initial conformation cannot be arbitrarily chosen.

Obviously, it must be emphasised that the qualitative aspect of this information could also have been extracted from looking at the original data related to the dimensions, i.e. 'X_{11}' vs 'X_{22}', plotted in Fig. 5b. In such plots, one would need to look at the gradients to assess the sign of the instantaneous Poisson's ratio and the relative positions between two points to assess the sign of the engineering/true Poisson's ratios. More specifically, for the 'instantaneous Poisson's ratio', a positive gradient in the 'dimensions' plot would indicate auxeticity, a zero gradient would indicate a zero Poisson's ratio

Table 2 The dimensions of the system (in mm) in Fig. 5 together with the strains and Poisson's ratio computed. System A is considered as the initial structure

	Dimensions		Strains in *y*-direction			Strains in *x*-direction			Poisson's ratio ν_{21}		
	X_{22}	X_{11}	e_2^{eng}	$\delta\varepsilon_2$	e_2^{true}	e_2^{eng}	$\delta\varepsilon_2$	e_2^{true}	Eng.	Instant	True
A	30	25									
B	34	22	0.133	0.133	0.125	-0.120	-0.120	-0.128	0.900	0.900	1.021
C	38	17	0.267	0.118	0.236	-0.320	-0.227	-0.386	1.200	1.932	1.631
D	42	17	0.400	0.105	0.336	-0.320	0.000	-0.386	0.800	0.000	1.146
E	46	23	0.533	0.095	0.427	-0.080	0.353	-0.083	0.150	-3.706	0.195
F	50	25	0.667	0.087	0.511	0.000	0.087	0.000	0.000	-1.000	0.000
G	54	28	0.800	0.080	0.588	0.120	0.120	0.113	-0.150	-1.500	-0.193
H	58	31	0.933	0.074	0.659	0.240	0.107	0.215	-0.257	-1.446	-0.326
I	62	27	1.067	0.069	0.726	0.080	-0.129	0.077	-0.075	1.871	-0.106

whilst a negative gradient would indicate positive Poisson's ratio. Similarly, the sign of the engineering/true Poisson's ratio can be worked out from the gradient of the line joining two datapoints, one of which should be the original system.

The Poisson's ratio properties of hexagonal honeycombs

Applying the method presented above, for the honeycomb system for loading in the vertical Ox_2 or horizontal Ox_1 direction, one obtains the following:

(1) Engineering strains and engineering Poisson's ratio:

$$e_1^{eng}(\theta) = \frac{\sin(\theta) - \sin(\theta_0)}{\sin(\theta_0)}$$

$$e_2^{eng}(\theta) = -\frac{l\cos(\theta) - l\cos(\theta_0)}{h - l\cos(\theta_0)} = -\frac{\cos(\theta) - \cos(\theta_0)}{h/l - \cos(\theta_0)}$$

$$\nu_{21}^{eng} = \left(\nu_{12}^{eng}\right)^{-1} = -\frac{e_1^{eng}}{e_2^{eng}} = \frac{\sin(\theta) - \sin(\theta_0)}{\cos(\theta) - \cos(\theta_0)}\frac{h/l - \cos(\theta_0)}{\sin(\theta_0)}$$

(2) Infinitesimally small strains and Poisson's function:

$$d\varepsilon_1(\theta) = \frac{dX_{11}}{X_{11}} = \frac{1}{X_{11}}\frac{dX_{11}}{d\theta}d\theta = \frac{2l\cos(\theta)}{2l\sin(\theta)}d\theta = \frac{\cos(\theta)}{\sin(\theta)}d\theta = \cot(\theta)d\theta$$

$$d\varepsilon_2(\theta) = \frac{dX_{11}}{X_{11}} = \frac{1}{X_{11}}\frac{dX_{11}}{d\theta}d\theta = \frac{2l\sin(\theta)}{2h - 2l\cos(\theta)}d\theta = \frac{\sin(\theta)}{h/l - \cos(\theta)}d\theta$$

$$\nu_{21} = (\nu_{12})^{-1} = -\frac{d\varepsilon_1}{d\varepsilon_2} = -\frac{(h/l - \cos(\theta))\cos(\theta)}{\sin^2(\theta)}$$

(3) True strains and true Poisson's ratio:

$$e_1^{true}(\theta) = \ln\left(\frac{X_{11}(\theta)}{X_{11}(\theta_o)}\right) = \ln\left(\frac{2l\sin(\theta)}{2l\sin(\theta_o)}\right) = \ln\left(\frac{\sin(\theta)}{\sin(\theta_o)}\right) = \ln(\sin(\theta)) - \ln(\sin(\theta_o))$$

$$e_2^{true}(\theta) = \ln\left(\frac{X_{22}(\theta)}{X_{22}(\theta_o)}\right) = \ldots = \ln\left(\frac{h/l - \cos(\theta)}{h/l - \cos(\theta_o)}\right) = \ln(h/l - \cos(\theta)) - \ln(h/l - \cos(\theta_o))$$

$$\nu_{21}^{true} = \left(\nu_{12}^{true}\right)^{-1} = -\frac{e_1^{true}}{e_2^{true}} = -\frac{\ln(\sin(\theta)) - \ln(\sin(\theta_o))}{\ln(h/l - \cos(\theta)) - \ln(h/l - \cos(\theta_o))}$$

It should be noted that, due to physical constraints, if the structure had to be loaded in tension in the horizonal Ox_1 direction, the system would not have been able to go past the 90° conformation (T-shaped joints) through the hinging mechanism as this would represent a locking position. There are no such locking positions for loading in the vertical Ox_2 direction (apart from the extreme conformations were $\theta = 0^o$ or $\theta = 180^o$).

Typical results for the hexagonal honeycombs where $l = 1$ and $h = 2$ (i.e. as in Fig. 6 below) are reported through plots of the unit cell lengths, plotted against each other and against θ (Fig. 7), as well as the so derived Poisson's ratio plotted against the applied engineering strain and the angle θ for the systems (Fig. 8). These plots were produced for various initial conformations of the honeycomb which include the ones where honeycombs are almost fully closed. In the case of the true Poisson's ratio, this is also plotted against the applied true strain.

The Poisson's ratio properties of the type I rotating rectangles

Using the procedure described above, the strains and Poisson's ratios for the 'rotating rectangles' system may be expressed as follows:

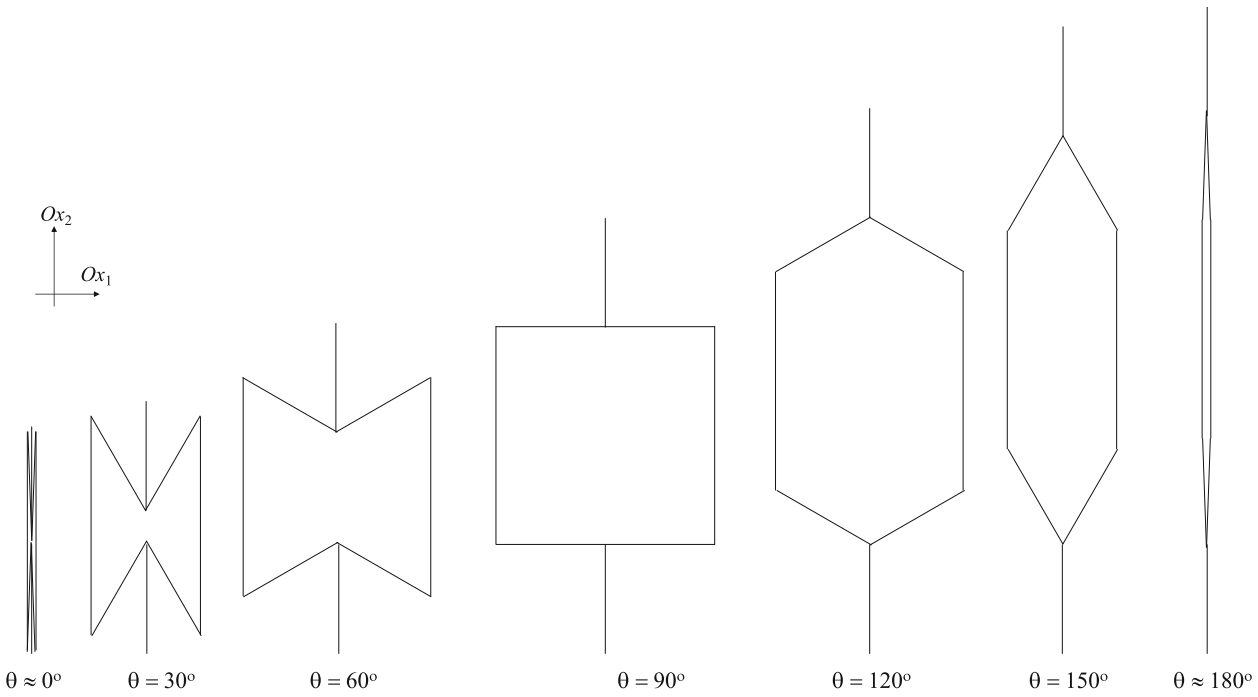

Fig. 6 To-scale representation of the hinging honeycombs with $h = 2$, $l = 1$ as these are stretched/compressed in the vertical or horizontal direction. Note that systems where $\theta < 90^{o}$ cannot be pulled in the horizontal direction past the system where $\theta = 90^{o}$ to achieve $\theta > 90^{o}$ whilst the systems where $\theta > 90^{o}$ cannot be pulled in the horizontal direction past the system where $\theta = 90^{o}$ to achieve $\theta < 90^{o}$, i.e. $\theta = 90^{o}$ corresponds to a 'locking conformation' for pulling in the horizontal direction

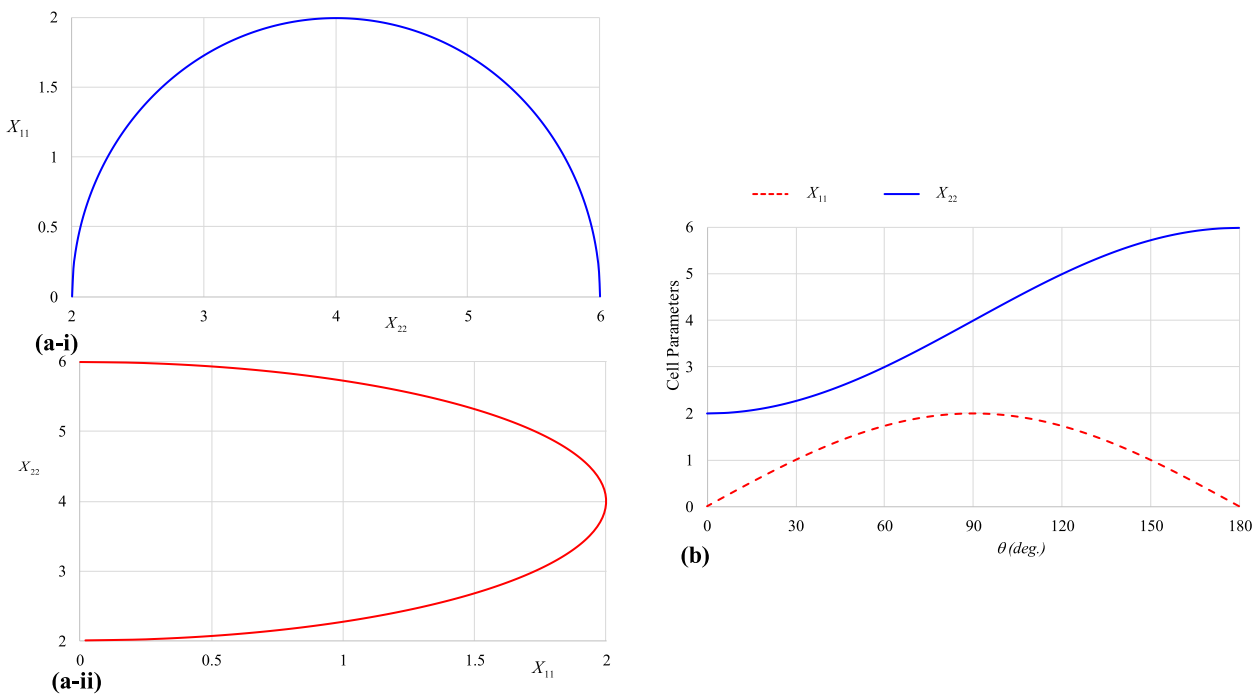

Fig. 7 a The cell parameters for the honeycombs plotted against each other. **b** The cell parameters plotted against the parameter θ. Note that the plot in (a-i) would be most useful for loading in Ox_2 whilst that in (a-ii) for loading in Ox_1, where the turning point corresponds to the locked conformation ($\theta = 90^{0}$) and the lower portion refers to angles less than 90^{0} whilst the upper portion refers to angles more than 90^{0}

$$\nu_{21}^{eng} = \left(\nu_{12}^{eng}\right)^{-1} = -\frac{\left[a\cos\left(\frac{\theta}{2}\right)+b\sin\left(\frac{\theta}{2}\right)-a\cos\left(\frac{\theta_0}{2}\right)-b\sin\left(\frac{\theta_0}{2}\right)\right]\left[b\cos\left(\frac{\theta_0}{2}\right)+a\sin\left(\frac{\theta_0}{2}\right)\right]}{\left[b\cos\left(\frac{\theta}{2}\right)+a\sin\left(\frac{\theta}{2}\right)-b\cos\left(\frac{\theta_0}{2}\right)-a\sin\left(\frac{\theta_0}{2}\right)\right]\left[a\cos\left(\frac{\theta_0}{2}\right)+b\sin\left(\frac{\theta_0}{2}\right)\right]}$$

(1) Engineering strains and engineering Poisson's ratio:

$$e_1^{eng}(\theta) = \frac{a\cos\left(\frac{\theta}{2}\right)+b\sin\left(\frac{\theta}{2}\right)-a\cos\left(\frac{\theta_0}{2}\right)-b\sin\left(\frac{\theta_0}{2}\right)}{a\cos\left(\frac{\theta_0}{2}\right)+b\sin\left(\frac{\theta_0}{2}\right)}$$

$$e_2^{eng}(\theta) = \frac{b\cos\left(\frac{\theta}{2}\right)+a\sin\left(\frac{\theta}{2}\right)-b\cos\left(\frac{\theta_0}{2}\right)-a\sin\left(\frac{\theta_0}{2}\right)}{b\cos\left(\frac{\theta_0}{2}\right)+a\sin\left(\frac{\theta_0}{2}\right)}$$

(2) Infinitesimally small strains and Poisson's function:

$$d\varepsilon_1(\theta) = \frac{-a\sin\left(\frac{\theta}{2}\right)+b\cos\left(\frac{\theta}{2}\right)}{2a\cos\left(\frac{\theta}{2}\right)+2b\sin\left(\frac{\theta}{2}\right)}$$

$$d\varepsilon_2(\theta) = \frac{a\cos\left(\frac{\theta}{2}\right)-b\sin\left(\frac{\theta}{2}\right)}{2a\sin\left(\frac{\theta}{2}\right)+2b\cos\left(\frac{\theta}{2}\right)}$$

$$\nu_{21}^{f} = \left(\nu_{12}^{f}\right)^{-1} = -\frac{\left[a\sin\left(\frac{\theta}{2}\right)+b\cos\left(\frac{\theta}{2}\right)\right]\left[-a\sin\left(\frac{\theta}{2}\right)+b\cos\left(\frac{\theta}{2}\right)\right]}{\left[a\cos\left(\frac{\theta}{2}\right)+b\sin\left(\frac{\theta}{2}\right)\right]\left[a\cos\left(\frac{\theta}{2}\right)-b\sin\left(\frac{\theta}{2}\right)\right]} = \frac{a^2\sin^2\left(\frac{\theta}{2}\right)-b^2\cos^2\left(\frac{\theta}{2}\right)}{a^2\cos^2\left(\frac{\theta}{2}\right)-b^2\sin^2\left(\frac{\theta}{2}\right)}$$

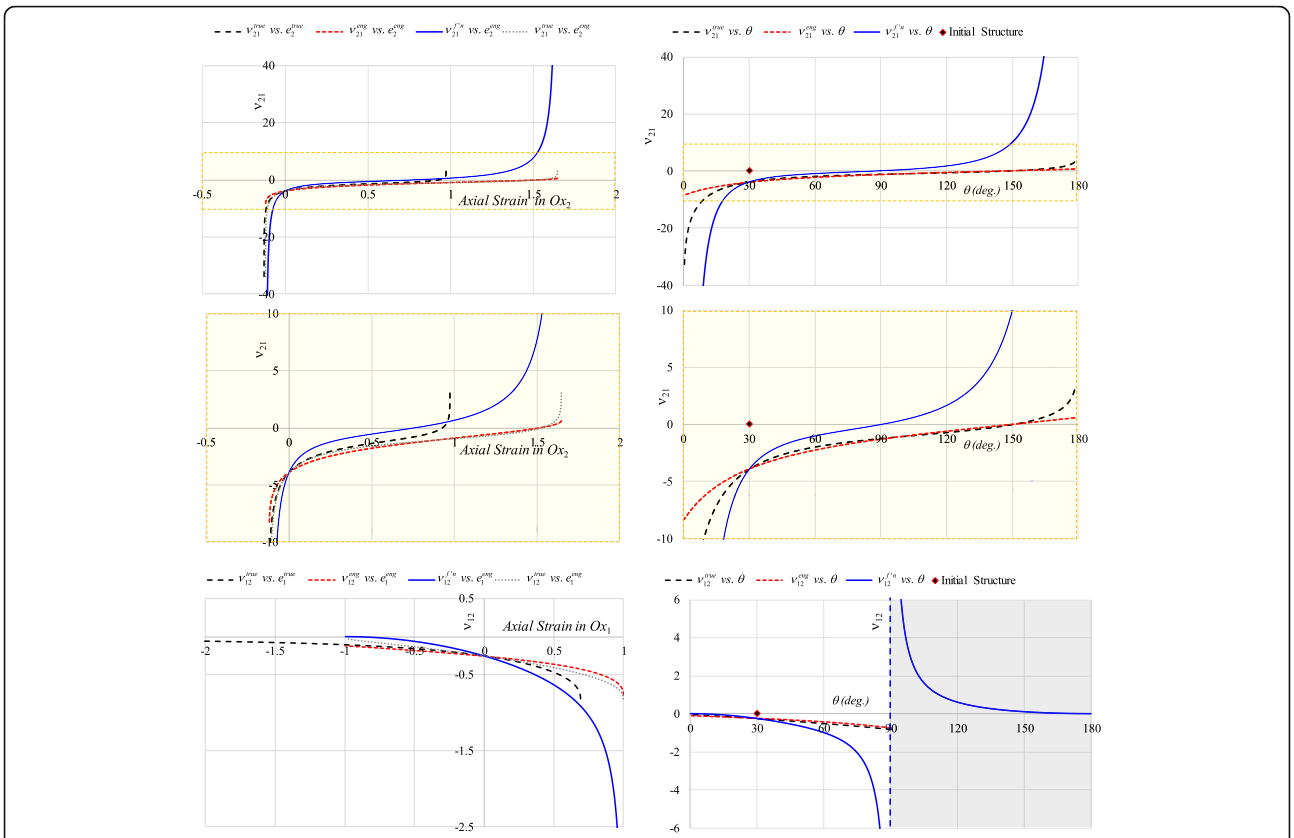

Fig. 8 Plots of the Poisson's ratios for honeycombs having $h = 2$, $l = 1$ for an initial configuration having an angle between the ligaments of $\theta_o = 30^\circ$ plotted against strain (left) and against the angle θ (right). The shaded region (grey) highlights a non-accessible range of angles. Note that in the case of axial straining in the Ox_2 direction, a second set of plots is presented which highlights a smaller range of Poisson's ratios

(3) True strains and true Poisson's ratio:

$$\varepsilon_1^{true}(\theta) = \ln\left[\frac{a\cos\left(\frac{\theta}{2}\right)+b\sin\left(\frac{\theta}{2}\right)}{a\cos\left(\frac{\theta_0}{2}\right)+b\sin\left(\frac{\theta_0}{2}\right)}\right]$$

$$\varepsilon_2^{true}(\theta) = \ln\left[\frac{b\cos\left(\frac{\theta}{2}\right)+a\sin\left(\frac{\theta}{2}\right)}{b\cos\left(\frac{\theta_0}{2}\right)+a\sin\left(\frac{\theta_0}{2}\right)}\right]$$

$$\nu_{21}^{true} = \left(\nu_{12}^{true}\right) = -\frac{\ln\left[\frac{a\cos\left(\frac{\theta}{2}\right)+b\sin\left(\frac{\theta}{2}\right)}{a\cos\left(\frac{\theta_0}{2}\right)+b\sin\left(\frac{\theta_0}{2}\right)}\right]}{\ln\left[\frac{b\cos\left(\frac{\theta}{2}\right)+a\sin\left(\frac{\theta}{2}\right)}{b\cos\left(\frac{\theta_0}{2}\right)+a\sin\left(\frac{\theta_0}{2}\right)}\right]}$$

Note that in this case, as amply discussed elsewhere (Grima et al., 2004; Grima, Alderson, & Evans, 2005), there are locking conformations which correspond to the conformations when the diagonals of rectangular units become aligned to the direction of loading. As shown in Fig. 9, for loading in the Ox_2 direction, these angles correspond to $2\phi_2 + \theta_{m2} = 180^o$ where $\phi_2 = \tan^{-1}\left(\frac{b}{a}\right)$ whilst for loading in Ox_1 direction, they correspond to $2\phi_1 + \theta_{m1} = 180^o$ where $\phi_1 = \tan^{-1}\left(\frac{a}{b}\right)$. Thus, for this specific case where loading is in the Ox_2 direction, if the original structure has an angle between the rectangles of θ_0, where $0^o < \theta_0 < \theta_{m2}$, then the system cannot be stretched past $\theta = \theta_{m2}$, at which angle, X_{22} is at a maximum. Similarly, for $\theta_{m2} < \theta_0 < 180^o$. The practical relevance of these conformations may be appreciated better in Fig. 10 below which shows a to-scale representation of the rotating rectangles model were a = 2 and b = 1. This image also visually highlights the typical Poisson's ratio properties of these systems.

General discussion

The intention of this discussion will not be to focus on the ability of these systems to exhibit negative Poisson's ratios as such properties are amply documented (Abd El-Sayed et al., 1979; Evans et al., 1995; Gibson et al., 1982; Grima et al., 2004; Grima, Alderson, & Evans, 2005; Masters & Evans, 1996). Instead, the focus will be to discuss the appropriateness of the various Poisson's ratios to represent what is really happening as the systems are being stretched or compressed. To do this, it is important to interpret the plots of the Poisson's ratios in conjunction with the images depicting the systems and the plots of the unit cell parameters.

Looking at the honeycomb systems shown in Fig. 6, without loss of generality, the discussion will first focus on the properties when the starting conformation is a re-entrant honeycomb having a geometry where the

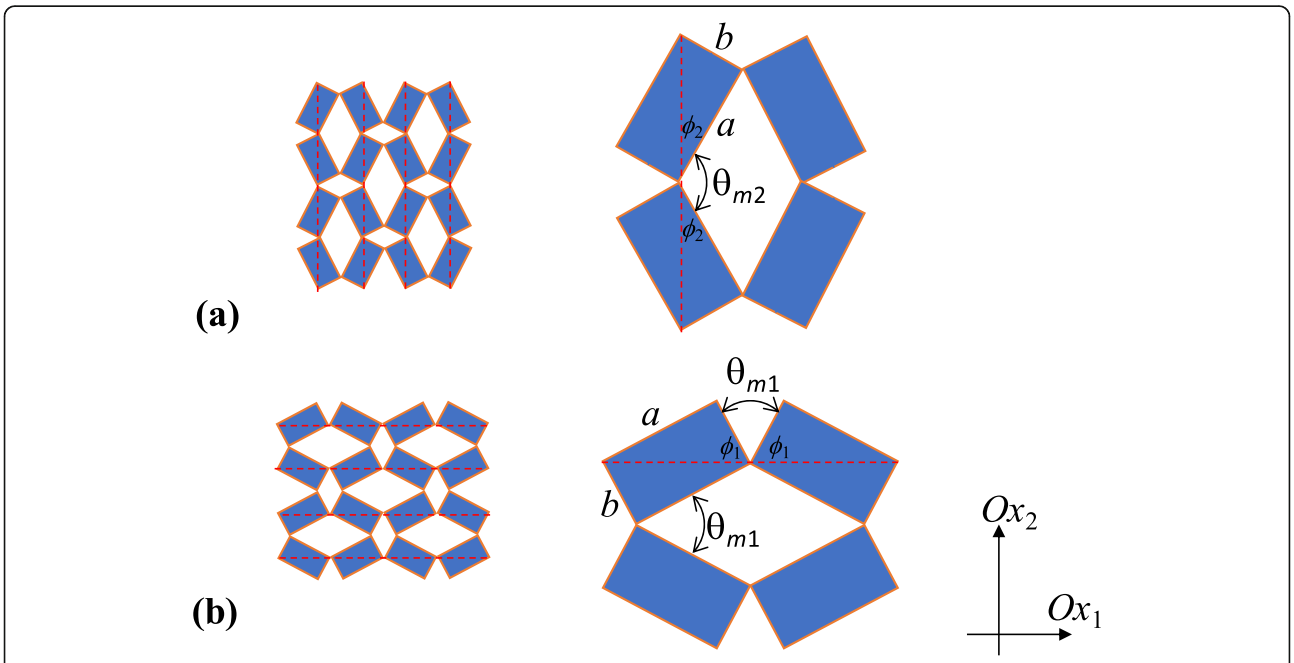

Fig. 9 The 'locking conformations' of the type I rotating rectangles system as this is stretched in **a** the Ox_2 direction and **b** the Ox_1 direction. Note that locking occurs when diagonals of rectangular units become parallel to the direction of loading as this would correspond to the most stretched conformation in that direction

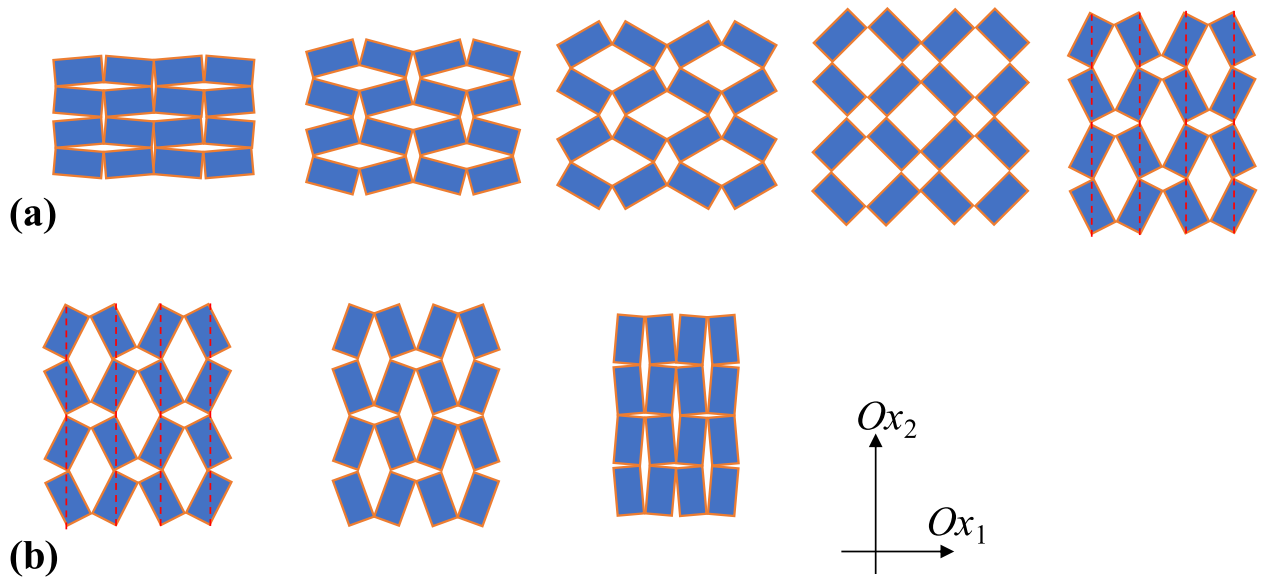

Fig. 10 To-scale representation of the rotating rectangles model were $a = 2$ and $b = 1$. Note that the different conformations in **a** correspond to $0^o < \theta < 126.87^o$ whilst those in **b** correspond to $126.87^o < \theta < 180^o$

initial angle between the ligaments is $\theta_0 = 30^o$. This is a representative dimension in the Ox_2 direction of $X_{22} \approx 2.27$ mm. Recognising that the representative dimensions in the Ox_2 direction can span from $X_{22} = 2.00$ mm (fully closed re-entrant system, $\theta = 0^o$) to $X_{22} = 6.00$ (fully closed non re-entrant system, $\theta = 180^o$), this corresponds to a structure which is very near to the fully closed re-entrant conformation. From the perspective of dimensions in the horizontal direction, $\theta_0 = 30^o$ corresponds to $X_{11} = 1.00$ mm, which corresponds to the median size, since in this case, the permissible range of values is between 0.00 mm (corresponding to the hypothetical fully closed system) and 2.00 mm (corresponding to the fully stretched structure with T-shaped joints). This suggests that this system can be compressed by *c.* 0.27 mm in the vertical direction, which would result in a massive horizontal contraction of almost ×4 this amount (*c.* 0.97) to become, at least in theory, negligibly thin. This situation for compressing in the vertical direction presents one of the classical dilemmas on the Poisson's ratio and how this should be reported. On the one hand, one could argue that the system is simply contracting by a finite amount when it is strained by another finite amount, resulting in a Poisson's ratio which obviously should be large in magnitude, but finite. Such a Poisson's ratio is reported through the engineering or true Poisson's ratio, which in this case is negative (as it should be) since the system is contracting laterally as it is compressed, and large in magnitude, reflecting the fact that the system shrinks laterally by a very substantial amount (see structures in Fig. 6). Nonetheless, one could equally argue that since this system becomes, theoretically, infinitely thin as it is axially compressed, reporting of a Poisson's ratio ν_{21} which tends to $-\infty$ would be merited. Such 'giant auxeticity' is only obtainable by the Poisson's function. Here, it should however be mentioned that the three formulations of the Poisson's ratio can be considered as relatively concordant at least when compared to other situations where the difference is much more pronounced. For example, if one looks at the same system when this is subjected to a tensile load in the vertical direction, one would notice that the three versions of the Poisson's ratios differ substantially from each other, even in sign. The 'true' and 'engineering' Poisson's ratios seem to suggest that auxetic behaviour is retained till the system is stretched from 0% strain ($\theta_0 = 30^o$) till reaching an engineering strain of *c.* 1.50, representing an axial extension of *c.* 150% ($\theta = 150^o$, which is almost the fully stretched conformation in Ox_2 direction). This tallies with the observation that if one had to compare a 'before' and 'after' scenario, there is always an evident widening upon stretching compared to the initial system. As noted above, from a practical perspective, this extensive widening compared to the initial system is an important result since in a number of practical situations, it is these 'before' and 'after' states which are of utmost importance, and not the path undertaken during the deformation. On the other hand, if knowledge of Poisson's ratio during the deformation path is required, for example, in applications where the sample needs to be "seen" getting fatter as it is

stretched, then the only usable 'auxetic' portion of the deformation would be till stretching by *c.* 76% ($e_2^{eng} \approx 0.76$, $\theta = 90^o$) as it is only till that conformation that the sample is visibly getting wider, following which it would start to contract again (see Fig. 6), as expected, since such honeycombs are not re-entrant. This information is only extractable from the Poisson's function.

It is sometimes also equally important to have knowledge of the Poisson's ratio at some particular extent of deformation. For example, if the application is such that the system needs to be initially deformed, and after this deformation, the Poisson's ratio of the 'stretched (or compressed) sample' would still need to be negative, then the Poisson's function would need to be considered. A practical example of this is in the use of auxetics for the manufacture of insoles where, to be able to benefit from the advantages associated with auxeticity, the sample needs to retain the auxeticity after contracting due to the effect of the bodyweight of the individual.

All this may suggest that the Poisson's function offers the most advantages compared to other methods of reporting the Poisson's ratio. However, the results reported here also suggest that the formulation of Poisson's function is rather inadequate to describe the behaviour of systems which approach a 'locking conformation'. This can be very clearly seen by looking at the results for loading in the horizontal direction where the Poisson's function seems to suggest that the system should be exhibiting giant auxeticity as it is approaching the $\theta = 90^o$ conformation. Nevertheless, when looking at the conformations in Fig. 6, this supposedly giant auxeticity is not easy to detect. In fact, an analysis of the deformations clearly suggests that there is nothing remarkable as the system is stretched on approaching $\theta = 90^o$ ($e_1^{eng} \rightarrow 1.00$) with the engineering and true Poisson's ratio reporting a more modest value of − 0.76 and − 0.82, respectively, which is more in line with what is being observed. The artificial report of 'giant auxeticity' as $e_1^{eng} \rightarrow 1.00$ may be explained by the fact that the expression for the Poisson's function involves a division by 0, since in the following:

$$\nu_{12}^{f'n}(\theta) = -\frac{d\varepsilon_2(\theta)}{d\varepsilon_1(\theta)} = -\frac{X_{22}}{X_{11}}\left(\frac{dX_{22}}{d\theta}\right)\left(\frac{dX_{11}}{d\theta}\right)^{-1}$$

$\frac{dX_{11}}{d\theta} = \cos(\theta) = 0$ when $\theta = 90^o$, a maximum turning point in the plot of X_{11} *vs.* θ.

Unfortunately, from a physical perspective this corresponds to a 'locking conformation' (i.e. a point where deformation becomes blocked) and not one where the system gets very significantly thicker as it is stretched, and hence one may conclude that this report of supposedly 'giant auxeticity' is a mere artefact of the method used rather than a real effect. All these emphasise that no formulation of the Poisson's ratio that have been formulated so far can be considered as being optimal.

Focusing the attention on the results obtained when the starting conformation is a re-entrant honeycomb where the initial angle between the ligaments is $\theta_0 = 1.00^o$, i.e. a re-entrant conformation which is practically fully closed and almost infinitly thin, differences between the output of the different formulations, and some other inadequacies, come to light. Looking first at stretching in the vertical direction, with this starting conformation, the system can be stretched from a practically infinitely thin conformation (re-entrant) to another practically infinitely thin conformation (the non-re-entrant, where $\theta \rightarrow 180^o$, $e_1^{eng} \rightarrow 2.00$) with the widest conformation being mid-way through the deformation when $\theta = 90^o$ ($e_1^{eng} = 1.00$). Here, the three formulations of the Poisson's ratio differ significantly from each other with the engineering form predicting giant auxeticity over most of the range of stretching (even when the thickness is actually decreasing) to describe the fact that, compared with the initial system, the width of the stretched system would always have increased by orders of magnitude thus becoming very noticeably wider when compared to the practically infinitly thin initial conformation. From this perspective, it is the engineering Poisson's ratio which highlights best the giant auxeticity, and, as noted before, the Poisson's function reports the Poisson's ratio as it varies along the path, changing sign from negative to positive mid-way when $\theta = 90^o$. However, in this case, the most remarkable differences can be spotted when stretching in the Ox_1 horizontal direction where the engineering Poisson's ratio reports near zero negative values almost throughout the deformation whilst the Poisson's function reports a much larger negative value which tends to $-\infty$ as the system approaches the 'locking conformation' when $\theta = 90^o$. In analogy to what was discussed before, such giant auxeticity is just an artefact of the method rather than a massive expansion upon stretching. What needs to be considered well is the report of the near zero engineering Poisson's ratios, which brings its own niche of importance and practical applications (Attard & Grima, 2011; Gaal, Rodrigues, Dantas, Galvão, & Fonseca, 2020; Grima et al., 2010). One could argue that the observed increase in size in the Ox_2 direction upon stretching in the Ox_1 direction is not insignificant (i.e. the magnitude of the Poisson's ratio should not be too low). However, one could equally argue that over most of the deformation, this increase in width is practically insignificant when compared to the manifold increase in size that is experienced in the direction of stretching (Ox_1), i.e. a Poisson's ratio close to zero is justifiable. In fact, on closer observation of Fig. 6, one may note, for example, that as θ changes from 1 to 30°,

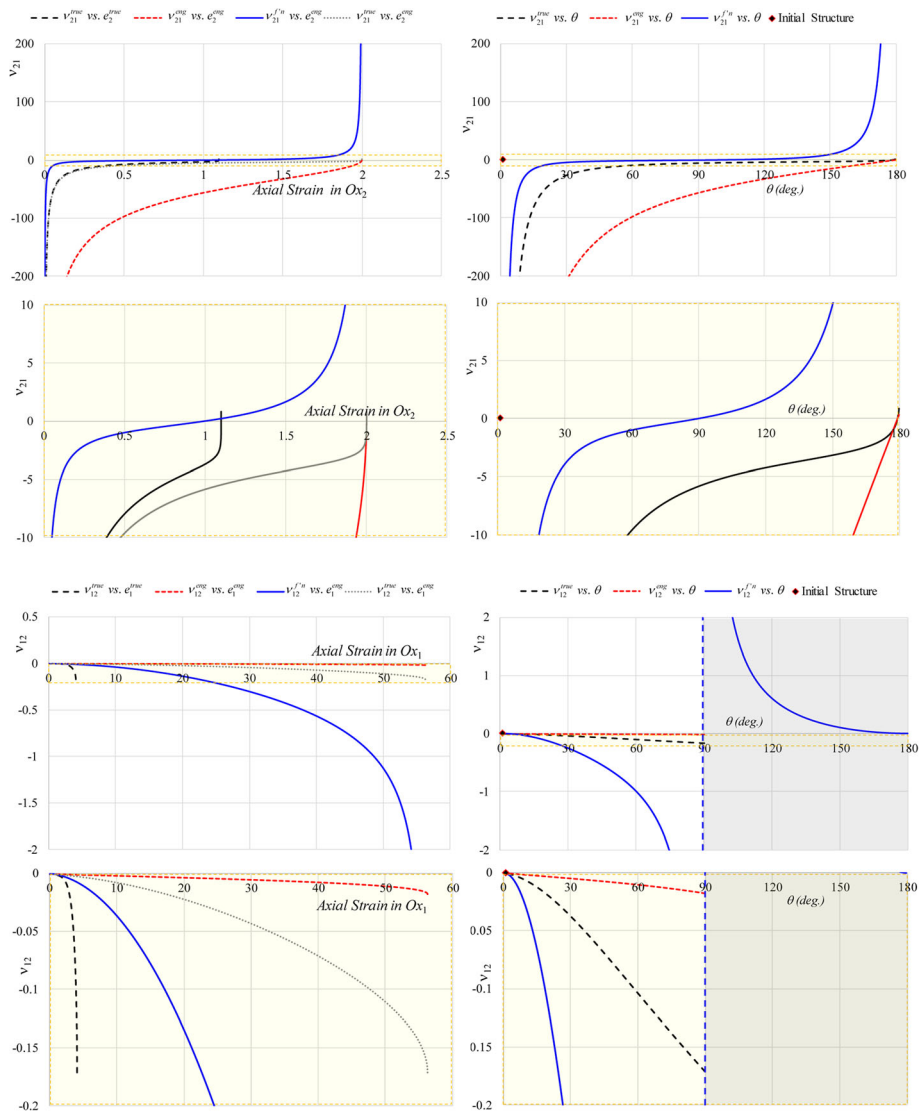

Fig. 11 Plots of the Poisson's ratios for honeycombs having $h = 2$, $l = 1$ for an initial configuration having an angle between the ligaments of $\theta_o = 1^o$ plotted against strain (left) and against the angle θ (right). The shaded region (grey) highlights a non-accessible range of angles. Note that a second set of plots is presented which highlights a smaller range of Poisson's ratios

although there is a gigantic increase in the length in the direction of stretching, the width only changes by a comparatively negligible amount from *c.* 2 to *c.* 2.27 (*c.* 10%.).

An obvious remark that should also be made at this point is that, in addition to what is stated above, an advantage of using the Poisson's function is that it is independent of the starting conformation, i.e. in some aspects, it is more amenable for discussion and reporting. In contrast, the engineering and true Poisson's ratios are highly dependent on the initial conformation, as evident when one compares Figs. 8, 11, and 12, which consider systems with a different initial conformation, including one where the initial conformation is not re-entrant, from which plots similar conclusions to those discussed above can be drawn.

At this point, it should be remarked that the findings on the differences between the forms of the Poisson's ratios as reported for the hexagonal honeycomb are also transferable to other systems. To show this, similar plots are also reported for the type I rotating rectangles with $a = 2$ and $b = 1$ (as drawn to scale in Fig. 10) where the initial conformation has $\theta_0 = 20^o$ and $\theta_0 = 160^o$ (see Fig. 13). Note that when the rectangles have these dimensions, the locking angle for uniaxial loading in the Ox_2 direction is $\theta_{m2} = 126.87^o$, i.e. the system with $\theta_0 = 20^o$ can be operated through stretching/compression in the Ox_2 direction within the range $0^o < \theta < 126.87^o$ whilst the system with

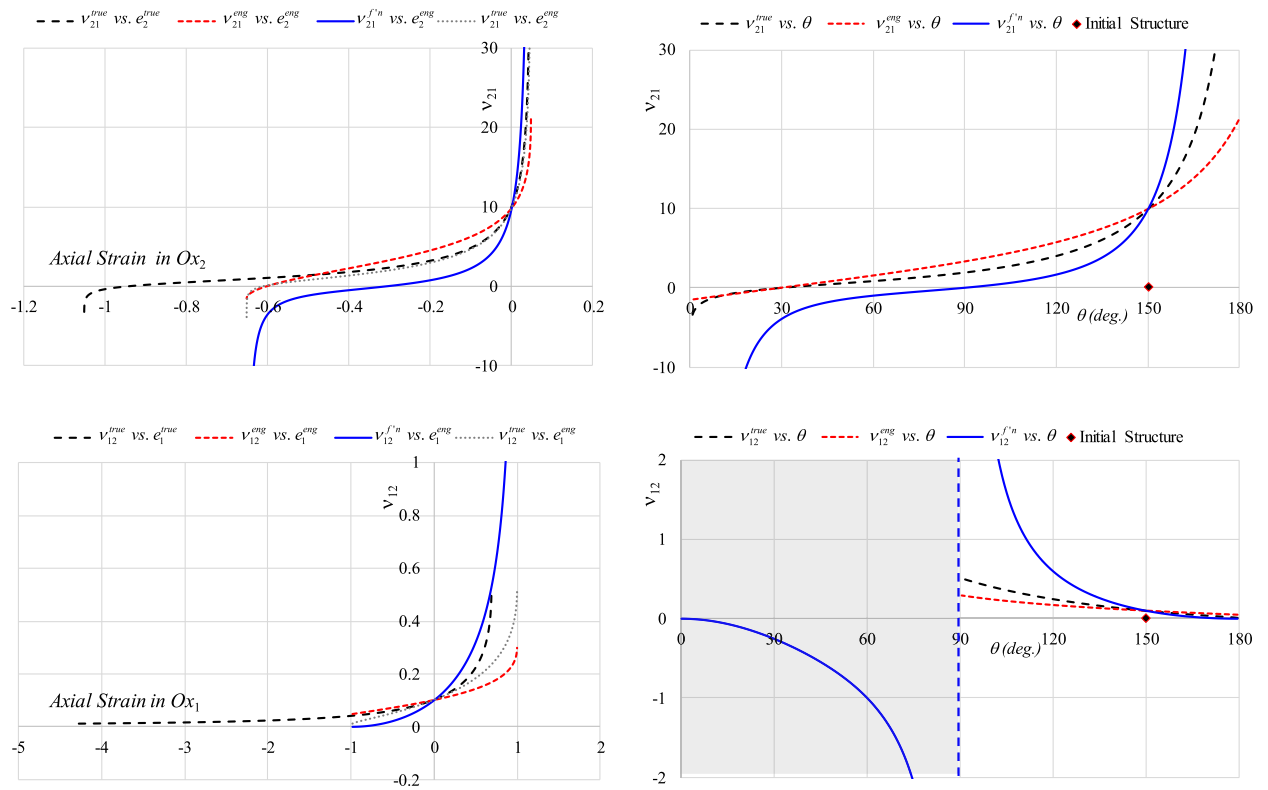

Fig. 12 Plots of the Poisson's ratios for honeycombs having $h = 2$, $l = 1$ for an initial configuration having an angle between the ligaments of $\theta_o = 150^o$ plotted against strain (left) and against the angle θ (right). This initial conformation is a non-re-entrant system and thus not auxetic at small strains. The shaded region (grey) highlights a non-accessible range of angles

$\theta_0 = 160^o$ can be similarly operated within the range $126.87^o < \theta < 180^o$, see Fig. 11. Note that at $\theta = 126.87^o$, the system would be at its maximum dimensions in the Ox_2 direction. As was the case for the honeycombs, an important conclusion that can be drawn is that the Poisson's function reported artificially large magnitudes of the Poisson's ratio as the system approached a locking conformation whilst the engineering and true Poisson's ratio formulations reported more realistic values. On the other hand, the Poisson's function once again offered the advantage that it permitted to easily identify when a change in behaviour (from 'getting thinner' to 'getting fatter', or vice versa) was observed whilst the deformation was taking place.

Given these various observations about the strengths and weaknesses of the various forms of expressing the Poisson's ratio, it is rather difficult to conclude which form is the best descriptor of reality, but one can definitely conclude that caution should be taken when interpreting any results. In view of this, it would be ideal if the report of the Poisson's ratio as the 'Poisson's function' (i.e. what is typically reported in analytical models (Alderson & Evans, 1995; Evans et al., 1995; Gatt, Attard, Manicaro, Chetcuti, & Grima, 2011; Grima & Evans, 2000; Grima, Gatt, et al., 2005) is complemented with either the report of the engineering or true Poisson's ratio, as was done in isolated cases (Alderson & Evans, 1995). An important remark that should be made is that the true Poisson's ratio formulation seems to avoid most of the 'extreme' reports of the Poisson's ratio. However, one must acknowledge that the true strains may be difficult to relate to the actual extent of deformation due to the use of the logarithmic function. For example, a 50% extension would correspond to a true strain of $\ln(1 + e) = \ln(1 + 0.5) \approx 0.405$, a value which is not of much 'meaning'. Thus, had one to opt to report the Poisson's ratio as a 'true Poisson's ratio', it would still be preferable to plot it against the more meaningful engineering strain, which could in itself lead to confusion in interpretation. Hence, from this aspect, the engineering Poisson's ratio is preferred over the true strain.

Before concluding, it must be noted that although this work has emphasised on the best way of reporting the Poisson's ratio, it must be stressed that the plots of the cell parameters themselves, which are generally not given much importance, contain a wealth of information in a very succinct manner. For example, when a load is

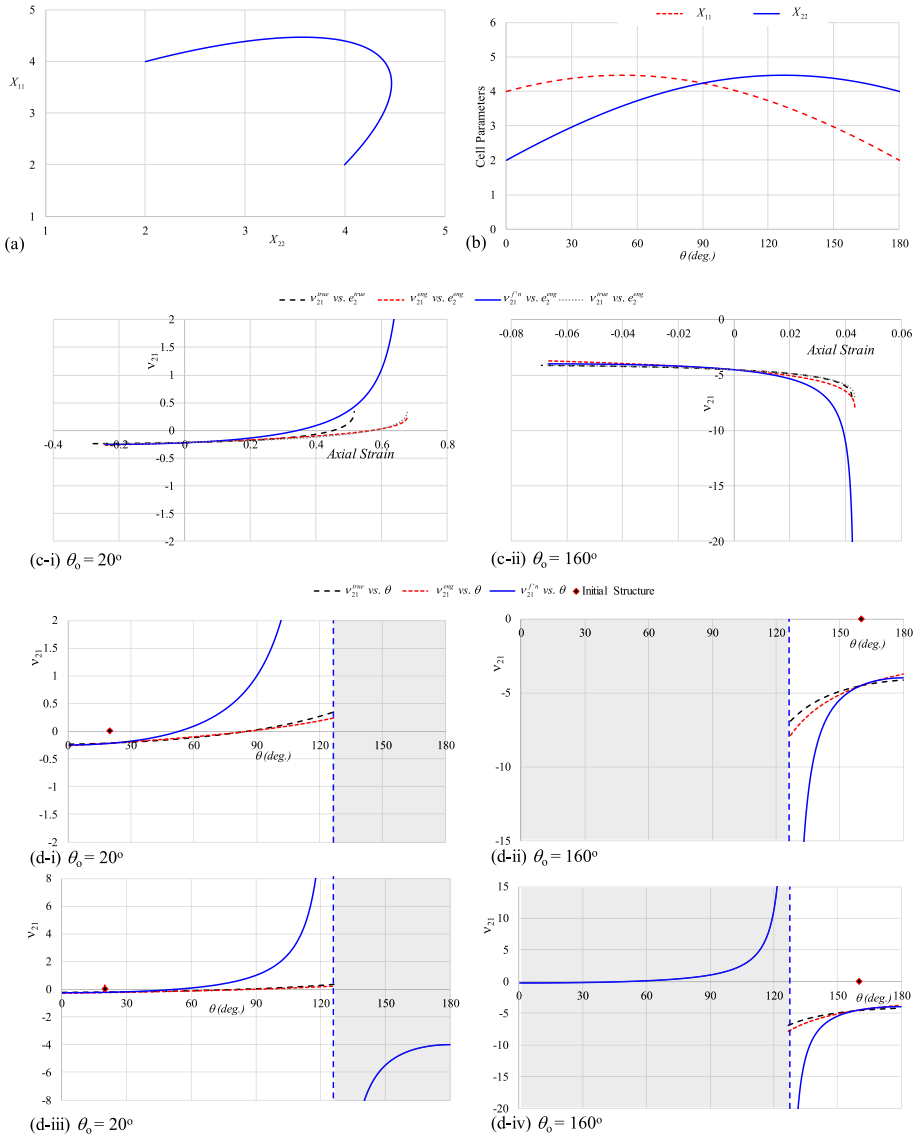

Fig. 13 Results for a typical type I rotating rectangles system with $a = 2$ and $b = 1$: **a** Plot of the cell parameters plotted against each other with X_{22} on the x-axis since this corresponds to the direction of loading. The 'loop' in this figure indicates the presence of a locked conformation; **b** the cell parameters plotted against the angle θ; **c** the Poisson's ratios plotted against applied strain in the Ox_2 direction for two different systems; **d** the Poisson's ratio plotted against the angular parameter θ where the shaded region indicates an inaccessible region. Plots (d-iii) and (d-iv) are equivalent to (d-i) and (d-ii) but with a larger range plotted

applied in the Ox_i direction, plots of X_{jj} *vs.* X_{ii} can yield the sign of the Poisson's function through the gradient, since from the following:

$$\nu_{ij}^{f'n}(\theta) = -\frac{d\varepsilon_j(\theta)}{d\varepsilon_i(\theta)} = -\frac{dX_{jj}/X_{jj}}{dX_{ii}/X_{ii}} = -\frac{X_{ii}}{X_{jj}}\frac{dX_{jj}}{dX_{ii}}$$

since X_{jj} and X_{ii} are always positive, a negative Poisson's ratio requires a positive gradient $\frac{dX_{jj}}{dX_{ii}}$. Furthermore, it should be noted that such plots can be used to easily identify locking conformations, as these are the conformations where the graph 'loops'. Here, it should be noted that whenever a graph of X_{jj} vs. X_{ii} 'loops' (as is the case in X_{22} vs. X_{11} for the hexagonal honeycombs), from a mathematical perspective, X_{jj} cannot be considered as a function of X_{ii}. This can, however, be considered as a proper function by only considering part of the data on a particular side of the locking conformation. The magnitude of the gradient of these plots also gives a very realistic measure of what one normally expects from a Poisson's ratio. Such data can usually be obtained from both modelling and experiment (it is normally the 'raw data'), and one may argue that it should become more standard practice to report it, possibly alongside the analysis of such data.

Conclusion

This work has compared the various ways how strain may be defined and how the actual definition affects the Poisson's ratio being computed. It was shown that different strain formulations result in rather different values and trends in the Poisson's ratio and that both the Poisson's ratio computed using the engineering strains and the ones obtained from the 'instantaneous strains' have their advantages and disadvantages.

In particular from this work, it was concluded that the various forms of determining the Poisson's ratio complement each other in describing the behaviour of systems which do not merely undergo infinitesimal deformations, particularly those which could exhibit both positive or negative Poisson's ratio (depending on the actual conformation, or extent of applied strain). It was thus concluded that the report of the Poisson's ratio should ideally be made both as the 'Poisson's function' and as the 'engineering/true Poisson's ratio'. A case was also made for reporting the actual 'sample' dimensions (or unit cell parameters) as these contain very useful and unbiased information which describe the Poisson's ratio of the system. It was argued that given that such data is normally easy to obtain from both modelling and experiment (the 'raw data'), it should become more standard practice to report it. Such more complete reporting of the Poisson's ratio behaviour would provide a more visually descriptive and unbiased picture of the true behaviour of auxetic systems and thus be of benefit to permit further research and development of systems studied computationally.

Abbreviations

Ox_i (i = 1,2,3): The mutually orthogonal Cartesian axis; ε_i (i = 1,2,3): Strain in the Ox_i direction (general definition); ν_{ij} (i,j = 1,2,3): Poisson's ratio in the Ox_i-Ox_j plane for loading in the Ox_i direction (general definition); e_i^{eng}

: Engineering strain in the Ox_i direction; e_i^{true}(i = 1,2,3): True strain in the Ox_i direction; $\delta\varepsilon_i$(i = 1,2,3): Incremental strain in the Ox_i direction; $d\varepsilon_i$: Infinitesimally small incremental strain in the Ox_i direction; ν_{ij}^{eng} (i,j = 1,2,3): Engineering Poisson's ratio in the Ox_i-Ox_j plane for loading in the Ox_i direction (computed from engineering strains); ν_{ij}^{true} (i,j = 1,2,3): True Poisson's ratio in the Ox_i-Ox_j plane for loading in the Ox_i direction (computed from engineering strains); $\nu_{ij}^{f'n}$ (i,j = 1,2,3): Poisson's function in the Ox_i-Ox_j plane for loading in the Ox_i direction (computed from incremental strains); **a**, **b**, **c**: Unit cell vectors; X_{ij} (i,j = 1,2,3): Component of the unit cell vectors, with X_{11} and X_{22} being the projections of the unit cell in Ox_1 and Ox_2 directions, respectively; L_{init}, L_{fin}: The initial and final length of a wire-like sample (defined in Fig. 1); $L[k]$, k = 0, 1, 2, 3, …: Successive length measures of a wire-like sample (defined in Fig. 1); $\delta L[k]$, k = 0, 1, 2, 3, …: Change in length between successive measurements in a wire-like sample between measurement k-1 and measurement k (defined in Fig. 1); $\mathbf{\Delta}L[k]$, k = 0, 1, 2, 3, …: Total change in length from the initial length to k^{th} measurement in a wire-like sample (defined in Fig. 1); l_1, l_2, h, θ_1, θ_2: Geometric parameters which define the shape of a generic hexagonal honeycomb (defined in Fig. 2); l, h, θ: Geometric parameters which define the shape of the more symmetric hexagonal honeycomb (defined in Fig. 2) where $l_1 = l_2 = l$ and $\theta_1 = \theta_2 = \theta$ throughout the deformation. For the hinging model discussed here, θ is a variable whilst the other parameters are constants; a, b, θ: Geometric parameters which define the shape of the rotating rectangles (defined in Fig. 4) For the hinging model discussed here, θ is a variable whilst the other parameters are constants.; θ_o: The value of θ for the initial structure; θ_m: A value of θ which corresponds to a 'locking position' (defined in Fig. 9 for rotating rectangles)

Acknowledgements

Not applicable.

Authors' contributions

JNGC conceived the work and produced the first draft of this manuscript. JNG edited the manuscript. DA supervised the project. All authors where involved in the discussion. The author(s) read and approved the final manuscript.

Funding

This work is funded by the University of Malta and the Malta Council for Science & Technology (A-ROW, a FUSION: The R&I Technology Development Programme 2018 project).

Availability of data and materials

All data generated or analysed during this study are included in this published article.

Competing interests

The authors declare that there are no competing interests.

Author details

[1]Metamaterials Unit, Faculty of Science, University of Malta, Msida MSD 2080, Malta. [2]Department of Chemistry, Faculty of Science, University of Malta, Msida MSD 2080, Malta.

Received: 18 July 2020 Accepted: 22 December 2020
Published online: 17 March 2021

References

Abd El-Sayed, F. K., Jones, R., & Burgess, I. W. (1979). A theoretical approach to the deformation of honeycomb based composite materials. *Composites*, *10*, 209–214. https://doi.org/10.1016/0010-4361(79)90021-1.

Alderson, A., Alderson, K. L., Evans, K. E., Grima, J. N., Williams, M. R., & Davies, P. J. (2005). Modelling the deformation mechanisms, structure-property relationships and applications of auxetic nanomaterials. *Physica Status Solidi B*, *242*, 499–508. https://doi.org/10.1002/pssb.200460370.

Alderson, A., & Evans, K. E. (1995). Microstructural modelling of auxetic microporous polymers. *Journal of Materials Science*, *30*, 3319–3332. https://doi.org/10.1007/BF00349875.

Alderson, K., Alderson, A., Ravirala, N., Simkins, V., & Davies, P. (2012). Manufacture and characterisation of thin flat and curved auxetic foam sheets. *Physica Status Solidi B*, *249*, 1315–1321. https://doi.org/10.1002/pssb.201084215.

Alderson, K. L., & Evans, K. E. (1992). The fabrication of microporous polyethylene having a negative Poisson's ratio. *Polymer*, *33*, 4435–4438. https://doi.org/10.1016/0032-3861(92)90294-7.

Allen, T., Duncan, O., Foster, L., Senior, T., Zampieri, D., Edeh, V., & Alderson, A. (2016). Auxetic foam for snow-sport safety devices. In *Snow Sport Trauma Saf Proc Int Soc Ski Saf*. https://doi.org/10.1007/978-3-319-52755-0_12.

Allen, T., Hewage, T., Newton-Mann, C., Wang, W., Duncan, O., & Alderson, A. (2017). Fabrication of auxetic foam sheets for sports applications. *Physica Status Solidi B*, *254*, 1700596. https://doi.org/10.1002/pssb.201700596.

Attard, D., & Grima, J. N. (2011). Modelling of hexagonal honeycombs exhibiting zero Poisson's ratio. *Physica Status Solidi B*, *248*, 52–59. https://doi.org/10.1002/pssb.201083980.

Attard, D., & Grima, J. N. (2012). A three-dimensional rotating rigid units network exhibiting negative Poisson's ratios. *Physica Status Solidi B*, *249*, 1330–1338. https://doi.org/10.1002/pssb.201084223.

Azzopardi, K. M., Brincat, J. P., Grima, J. N., & Gatt, R. (2015). Anomalous elastic properties in stishovite. *RSC Advances*, *5*, 8974–8980. https://doi.org/10.1039/c4ra12072h.

Babaee, S., Shim, J., Weaver, J. C., Chen, E. R., Patel, N., & Bertoldi, K. (2013). 3D soft metamaterials with negative Poisson's ratio. *Advanced Materials*, *25*, 5044–5049. https://doi.org/10.1002/adma.201301986.

Baughman, R. H., & Galvão, D. S. (1993). Crystalline networks with unusual predicted mechanical and thermal properties. *Nature*, *365*, 735–737. https://doi.org/10.1038/365735a0.

Bertoldi, K., Reis, P. M., Willshaw, S., & Mullin, T. (2010). Negative Poisson's ratio behavior induced by an elastic instability. *Advanced Materials*, *22*, 361–366. https://doi.org/10.1002/adma.200901956.

Brańka, A. C., Heyes, D. M., Makowiak, S., Pieprzyk, S., & Wojciechowski, K. W. (2012). Cubic materials in different auxetic regions: linking microscopic to macroscopic formulations. *Physica Status Solidi B*, *249*, 1373–1378. https://doi.org/10.1002/pssb.201084222.

Brańka, A. C., Heyes, D. M., & Wojciechowski, K. W. (2009). Auxeticity of cubic materials. *Physica Status Solidi B*, *246*, 2063–2071. https://doi.org/10.1002/pssb.200982037.

Brańka, A. C., Heyes, D. M., & Wojciechowski, K. W. (2011). Auxeticity of cubic materials under pressure. *Physica Status Solidi B*, *248*, 96–104. https://doi.org/10.1002/pssb.201083981.

Dudek, K. K., Wojciechowski, K. W., Dudek, M. R., Gatt, R., Mizzi, L., & Grima, J. N. (2018). Potential of mechanical metamaterials to induce their own global rotational motion. *Smart Materials and Structures*, *27*, 055007. https://doi.org/10.1088/1361-665X/aabbf6.

Dudek, K. K., Wolak, W., Dudek, M. R., Caruana-Gauci, R., Gatt, R., Wojciechowski, K. W., & Grima, J. N. (2017). Programmable magnetic domain evolution in magnetic auxetic systems. *Physica Status Solidi (RRL)*, *11*, 1700122. https://doi.org/10.1002/pssr.201700122.

Evans, K. E. (1991). Auxetic polymers: a new range of materials. *Endeavour*, *15*, 170–174. https://doi.org/10.1016/0160-9327(91)90123-S.

Evans, K. E., Alderson, A., & Christian, F. R. (1995). Auxetic two-dimensional polymer networks. An example of tailoring geometry for specific mechanical properties. *Journal of the Chemical Society, Faraday Transactions*, *91*, 2671–2680. https://doi.org/10.1039/ft9959102671.

Evans, K. E., Nkansah, M. A., Hutcherson, I. J., & Rogers, S. C. (1991). Molecular network design. *Nature*, *353*, 124. https://doi.org/10.1038/353124a0.

Fischer, D., & Eugster, A. (1994). *Espresso Machine. US5337652A*.

Gaal, V., Rodrigues, V., Dantas, S. O., Galvão, D. S., & Fonseca, A. F. (2020). New zero Poisson's ratio structures. *Physica Status Solidi (RRL)*, *14*, 1900564. https://doi.org/10.1002/pssr.201900564.

Gatt, R., Attard, D., Manicaro, E., Chetcuti, E., & Grima, J. N. (2011). On the effect of heat and solvent exposure on the microstructure properties of auxetic foams: a preliminary study. *Physica Status Solidi B*, *248*, 39–44. https://doi.org/10.1002/pssb.201083978.

Gibson, L. J., Ashby, M. F., Schajer, G. S., & Robertson, C. I. (1982). The mechanics of two-dimensional cellular materials. *Proc R Soc A Math Phys Eng Sci*, *382*, 25–42. https://doi.org/10.1098/rspa.1982.0087.

Greaves, G. N., Greer, A. L., Lakes, R. S., & Rouxel, T. (2011). Poisson's ratio and modern materials. *Nature Materials*, *10*, 823–837. https://doi.org/10.1038/nmat3134.

Grima, J. N., Alderson, A., & Evans, K. E. (2004). Negative Poisson's ratios from rotating rectangles. *Computational Methods in Science and Technology*, *10*, 137–145. https://doi.org/10.12921/cmst.2004.10.02.137-145.

Grima, J. N., Alderson, A., & Evans, K. E. (2005). Auxetic behaviour from rotating rigid units. *Physica Status Solidi B*, *242*, 561–575. https://doi.org/10.1002/pssb.200460376.

Grima, J. N., & Evans, K. E. (2000). Auxetic behavior from rotating squares. *Journal of Materials Science Letters*, *19*, 1563–1565. https://doi.org/10.1023/A:1006781224002.

Grima, J. N., Farrugia, P. S., Gatt, R., & Attard, D. (2008). On the auxetic properties of rotating rhombi and parallelograms: a preliminary investigation. *Physica Status Solidi B*, *245*, 521–529. https://doi.org/10.1002/pssb.200777705.

Grima, J. N., Gatt, R., Alderson, A., & Evans, K. E. (2006). An alternative explanation for the negative Poisson's ratios in α-cristobalite. *Materials Science and Engineering A*, *423*, 219–224. https://doi.org/10.1016/j.msea.2005.08.230.

Grima, J. N., Gatt, R., Alderson, A. E., & Evans, K. (2005). On the auxetic properties of 'rotating rectangles' with different connectivity. *Journal of the Physical Society of Japan*, *74*, 2866–2867. https://doi.org/10.1143/JPSJ.74.2866.

Grima, J. N., Grech, M. C., Grima-Cornish, J. N., Gatt, R., & Attard, D. (2018). Giant auxetic behaviour in engineered graphene. *Annalen der Physik*, *530*, 1700330. https://doi.org/10.1002/andp.201700330.

Grima, J. N., Jackson, R., Alderson, A., & Evans, K. E. (2000). Do zeolites have negative Poisson's ratios? *Advanced Materials*, *12*, 1912–1918 https://doi.org/10.1002/1521-4095(200012)12:24<1912::AID-ADMA1912>3.0.CO;2-7.

Grima, J. N., Manicaro, E., & Attard, D. (2011). Auxetic behaviour from connected different-sized squares and rectangles. *Proceedings of the Royal Society A: Mathematical, Physical and Engineering Sciences*, *467*, 439–458. https://doi.org/10.1098/rspa.2010.0171.

Grima, J. N., Oliveri, L., Attard, D., Ellul, B., Gatt, R., Cicala, G., & Recca, G. (2010). Hexagonal honeycombs with zero Poisson's ratios and enhanced stiffness. *Advanced Engineering Materials*, *12*, 855–862. https://doi.org/10.1002/adem.201000140.

Ha, C. S., Plesha, M. E., & Lakes, R. S. (2016). Chiral three-dimensional lattices with tunable Poisson's ratio. *Smart Materials and Structures*, *25*, 054005. https://doi.org/10.1088/0964-1726/25/5/054005.

Harkati, E., Daoudi, N., Bezazi, A., Haddad, A., & Scarpa, F. (2017). In-plane elasticity of a multi re-entrant auxetic honeycomb. *Composite Structures*, *180*, 130–139. https://doi.org/10.1016/j.compstruct.2017.08.014.

Hewage, T. A. M., Alderson, K. L., Alderson, A., & Scarpa, F. (2016). Double-negative mechanical metamaterials displaying simultaneous negative stiffness and negative Poisson's ratio properties. *Advanced Materials*, *28*, 10323–10332. https://doi.org/10.1002/adma.201603959.

Hoover, W. G., & Hoover, C. G. (2005). Searching for auxetics with DYNA3D and ParaDyn. *Physica Status Solidi B*, *242*, 585–594. https://doi.org/10.1002/pssb.200460377.

Ishibashi, Y., & Iwata, M. (2000). A microscopic model of a negative Poisson's ratio in some crystals. *Journal of the Physical Society of Japan*, *69*, 2702–2703. https://doi.org/10.1143/JPSJ.69.2702.

Juszkiewicz, H. E., & Ewen, A. J. (2002). *Audio speaker system for personal computer, WO200101549 2A1*.

Kadic, M., Tiemo, B., Schittny, R., & Wegener, M. (2013). Metamaterials beyond electromagnetism. *Reports on Progress in Physics*, *76*, 126501. https://doi.org/10.1088/0034-4885/76/12/126501.

Kolken, H. M. A., & Zadpoor, A. A. (2017). Auxetic mechanical metamaterials. *RSC Advances*, *7*, 5111–5129. https://doi.org/10.1039/C6RA27333E.

Lakes, R. (1987). Foam structures with a negative Poisson's ratio. *Science*, *235*, 1038–1040. https://doi.org/10.1126/science.235.4792.1038.

Lempriere, B. M. (1968). Poisson's ratio in orthotropic materials. *American Institute of Aeronautics and Astronautics Journal*, *6*, 2226–2227. https://doi.org/10.2514/3.4974.

Lim, T.-C. (2013). Circular auxetic plates. *Journal of Mechanics*, *29*, 121–133. https://doi.org/10.1017/jmech.2012.113.

Lim, T.-C. (2015). Simply-supported elliptical auxetic plates. *Journal of Mechanics*, *32*, 413–419. https://doi.org/10.1017/jmech.2015.102.

Liu, Y., & Hu, H. (2010). A review on auxetic structures and polymeric materials. *Scientific Research and Essays*, *5*, 1052–1063. https://doi.org/10.5897/SRE.9000104.

Mack, G. (2018). *Herzog & de Meuron Elbphilharmonie Hamburg*, (1st ed.,). Basel: Birkhäuser.

Mason, W. P. (1950). *Piezoelectric crystals and their application to ultrasonics*. New York: Van Nostrand.

Masters, I. G., & Evans, K. E. (1996). Models for the elastic deformation of honeycombs. *Composite Structures*, *35*, 403–422. https://doi.org/10.1016/S0263-8223(96)00054-2.

Milton, G. W. (2013). Complete characterization of the macroscopic deformations of periodic unimode metamaterials of rigid bars and pivots. *Journal of the Mechanics and Physics of Solids*, *61*, 1543–1560. https://doi.org/10.1016/j.jmps.2012.08.011.

Mizzi, L., Mahdi, E. M., Titov, K., Gatt, R., Attard, D., Evans, K. E., … Tan, J.-C. (2018). Mechanical metamaterials with star-shaped pores exhibiting negative and zero Poisson's ratio. *Materials and Design*, *146*, 28–37. https://doi.org/10.1016/j.matdes.2018.02.051.

Pandolfi, A. (1988). *Espresso Coffee Machine. US4757753A*.

Pasternak, E., & Dyskin, A. V. (2019). Architectured materials with inclusions having negative poisson's ratio or negative stiffness. In Y. Estrin, Y. Bréchet, J. Dunlop, & P. Fratzl (Eds.), *Architectured materials in nature and engineering*. Springer Series in Materials Science, (vol. 282). Cham: Springer. https://doi.org/10.1007/978-3-030-11942-3_3.

Poźniak, A. A., Wojciechowski, K. W., Grima, J. N., & Mizzi, L. (2016). Planar auxeticity from elliptic inclusions. *Composites. Part B, Engineering*, *94*, 379–388. https://doi.org/10.1016/j.compositesb.2016.03.003.

Qin, H., Sun, Y., Liu, J. Z., Li, M., & Liu, Y. (2017). Negative Poisson's ratio in rippled graphene. *Nanoscale*, *9*, 4135–4142. https://doi.org/10.1039/C6NR07911C.

Qu, J., Kadic, M., Naber, A., & Wegener, M. (2017). Micro-structured two-component 3D metamaterials with negative thermal-expansion coefficient from positive constituents. *Scientific Reports*, *7*, 40643. https://doi.org/10.1038/srep40643.

Russell, B. (1919). *Introduction to Mathematical Philosophy*, (1st ed.,). Dover: Dover Publications.

Ryder, M. R., & Tan, J.-C. (2016). Explaining the mechanical mechanisms of zeolitic metal–organic frameworks: revealing auxeticity and anomalous elasticity. *Dalton Transactions*, *45*, 4154–4161. https://doi.org/10.1039/C5DT03514G.

Sigmund, O. (1995). Tailoring materials with prescribed elastic properties. *Mechanics of Materials*, *20*, 351–368. https://doi.org/10.1016/0167-6636(94)00069-7.
Smith, C. W., Wootton, R. J., & Evans, K. E. (1999). Interpretation of experimental data for Poisson's ratio of highly nonlinear materials. *Experimental Mechanics*, *39*, 356–362. https://doi.org/10.1007/BF02329817.
Strek, T., Maruszewski, B. T., Narojczyk, J. W., & Wojciechowski, K. W. (2008). Finite element analysis of auxetic plate deformation. *Journal of Non-Crystalline Solids*, *354*, 4475–4480. https://doi.org/10.1016/j.jnoncrysol.2008.06.087.
Strek, T., Michalski, J., & Jopek, H. (2019). Computational analysis of the mechanical impedance of the sandwich beam with auxetic metal foam core. *Physica Status Solidi B*, *256*, 1–8. https://doi.org/10.1002/pssb.201800423.
Taylor, M., Francesconi, L., Gerendás, M., Shanian, A., Carson, C., & Bertoldi, K. (2014). Low porosity metallic periodic structures with negative Poisson's ratio. *Advanced Materials*, *26*, 2365–2370. https://doi.org/10.1002/adma.201304464.
Tretiakov, K. V., & Wojciechowski, K. W. (2014). Partially auxetic behavior in fcc crystals of hard-core repulsive Yukawa particles. *Physica Status Solidi B*, *251*, 383–387. https://doi.org/10.1002/pssb.201384244.
Verma, P., Shofner, M. L., & Griffin, A. C. (2014). Deconstructing the auxetic behavior of paper. *Physica Status Solidi B*, *251*, 289–296. https://doi.org/10.1002/pssb.201384243.
Verma, P., Shofner, M. L., Lin, A., Wagner, K. B., & Griffin, A. C. (2015). Inducing out-of-plane auxetic behavior in needle-punched nonwovens. *Physica Status Solidi B*, *252*, 1455–1464. https://doi.org/10.1002/pssb.201552036.
Wilson, R. H. J. (1964). The importance of mathematics in the Space Age The importance of mathematics in the Space Age. *Mathematics Teacher*, *57*, 290–297. https://doi.org/10.2307/27957049.
Wojciechowski, K. W. (1987). Constant thermodynamic tension Monte Carlo studies of elastic properties of a two-dimensional system of hard cyclic hexamers. *Molecular Physics*, *61*, 1247–1258. https://doi.org/10.1080/00268978700101761.
Wojciechowski, K. W. (1989). Two-dimensional isotropic system with a negative Poisson ratio. *Physics Letters A*, *137*, 60–64. https://doi.org/10.1016/0375-9601(89)90971-7.
Wojciechowski, K. W. (2003a). Non-chiral, molecular model of negative Poisson ratio in two dimensions. *Journal of Physics A: Mathematical and General*, *36*, 11765–11778. https://doi.org/10.1088/0305-4470/36/47/005.
Wojciechowski, K. W. (2003b). Remarks on "Poisson ratio beyond the limits of the elasticity theory.". *Journal of the Physical Society of Japan*, *72*, 1819–1820. https://doi.org/10.1143/JPSJ.72.1819.
Wojciechowski, K. W., Tretiakov, K. V., & Kowalik, M. (2003). Elastic properties of dense solid phases of hard cyclic pentamers and heptamers in two dimensions. *Physical Review E*, *67*, 36121. https://doi.org/10.1103/PhysRevE.67.036121.
Zhang, Z., Hu, H., Liu, S., & Xu, B. (2013). Study of an auxetic structure made of tubes and corrugated sheets. *Physica Status Solidi B*, *250*, 1996–2001. https://doi.org/10.1002/pssb.201248349.
Zheng, X., Lee, H., Weisgraber, T. H., Shusteff, M., DeOtte, J., Duoss, E. B., … Spadaccini, C. M. (2014). Ultralight, ultrastiff mechanical metamaterials. *Science*, *344*, 1373–1377. https://doi.org/10.1126/science.1252291.

Publisher's Note